International Journal of
Molecular Sciences

MDPI

Article

Intrinsic Lipid Curvature and Bilayer Elasticity as Regulators of Channel Function: A Comparative Single-Molecule Study

Mohammad Ashrafuzzaman [1,†], Roger E. Koeppe II [2] and Olaf S. Andersen [1,*]

[1] Department of Physiology and Biophysics, Weill Cornell Medicine, New York, NY 10065, USA; mzzaman@ksu.edu.sa
[2] Department of Chemistry and Biochemistry, University of Arkansas, Fayetteville, AR 72701, USA; rk2@uark.edu
* Correspondence: sparre@med.cornell.edu
† Present address: Department of Biochemistry, College of Science, King Saud University, Riyad 11451, Saudi Arabia.

Abstract: Perturbations in bilayer material properties (thickness, lipid intrinsic curvature and elastic moduli) modulate the free energy difference between different membrane protein conformations, thereby leading to changes in the conformational preferences of bilayer-spanning proteins. To further explore the relative importance of curvature and elasticity in determining the changes in bilayer properties that underlie the modulation of channel function, we investigated how the micelle-forming amphiphiles Triton X-100, reduced Triton X-100 and the H_{II} lipid phase promoter capsaicin modulate the function of alamethicin and gramicidin channels. Whether the amphiphile-induced changes in intrinsic curvature were negative or positive, amphiphile addition increased gramicidin channel appearance rates and lifetimes and stabilized the higher conductance states in alamethicin channels. When the intrinsic curvature was modulated by altering phospholipid head group interactions, however, maneuvers that promote a negative-going curvature stabilized the higher conductance states in alamethicin channels but destabilized gramicidin channels. Using gramicidin channels of different lengths to probe for changes in bilayer elasticity, we found that amphiphile adsorption increases bilayer elasticity, whereas altering head group interactions does not. We draw the following conclusions: first, confirming previous studies, both alamethicin and gramicidin channels are modulated by changes in lipid bilayer material properties, the changes occurring in parallel yet differing dependent on the property that is being changed; second, isolated, negative-going changes in curvature stabilize the higher current levels in alamethicin channels and destabilize gramicidin channels; third, increases in bilayer elasticity stabilize the higher current levels in alamethicin channels and stabilize gramicidin channels; and fourth, the energetic consequences of changes in elasticity tend to dominate over changes in curvature.

Keywords: lipid intrinsic curvature; elasticity; amphiphiles; bilayer-mediated regulation; gramicidin channel; alamethicin channel

Citation: Ashrafuzzaman, M.; Koeppe, R.E., II; Andersen, O.S. Intrinsic Lipid Curvature and Bilayer Elasticity as Regulators of Channel Function: A Comparative Single-Molecule Study. *Int. J. Mol. Sci.* **2024**, *25*, 2758. https://doi.org/10.3390/ijms25052758

Academic Editors: Marco Colombini and Sergey M. Bezrukov

Received: 6 January 2024
Revised: 13 February 2024
Accepted: 21 February 2024
Published: 27 February 2024

1. Introduction

Membrane protein function is regulated by changes in lipid bilayer composition [1–12]. This regulation is, in part, due to changes in membrane physical properties, including thickness (d_0), intrinsic lipid curvature (c_0), bilayer compression (K_a) and bending (K_c) moduli, e.g., [8]. The bilayer regulation of membrane protein function occurs because, first, membrane proteins undergo conformational changes; second, hydrophobic interactions between lipid bilayers and their embedded proteins cause bilayers to adapt to the proteins' hydrophobic exterior (and vice versa); and third, the hydrophobic adaptation between bilayers and proteins causes protein conformation changes to alter the packing in the adjacent bilayer. This bilayer deformation will incur an energetic cost that contributes to

the total free energy difference between two protein conformations (functional states), I and II ($\Delta G_{tot}^{I \to II}$), [8,13,14]:

$$\Delta G_{tot}^{I \to II} = \Delta G_{prot}^{I \to II} + \Delta G_{bil}^{I \to II} \quad (1)$$

where $\Delta G_{prot}^{I \to II}$ denotes the energetic cost of the rearrangements within the protein that underlie the protein conformational change and $\Delta G_{bil}^{I \to II}$ the bilayer contribution to $\Delta G_{tot}^{I \to II}$ ($\Delta G_{bil}^{I \to II} = \Delta G_{def}^{II} - \Delta G_{def}^{I}$, where ΔG_{def} denotes the energetic cost of the bilayer deformation (changes in organization and dynamics of the lipid molecules adjacent to the protein) caused by the hydrophobic adaptation to each protein conformation). ΔG_{def} varies as a function of d_0, c_0, K_a and K_c, and the protein's shape, including the hydrophobic length (l) [6,14,15], changes in any of these will alter $\Delta G_{bil}^{I \to II}$ and, thus, protein function.

Studies on purified proteins reconstituted in lipid bilayers of defined composition show that membrane protein function is altered by experimental maneuvers that alter bilayer thickness or lipid intrinsic curvature; for a review, see [6]. (In addition to changes in intrinsic curvature, membrane protein organization and function may also be modulated by changes in overall membrane curvature [16,17] in which the two interfaces have opposite curvatures; we will not consider such changes). It is generally accepted that the bilayer thickness-dependent changes in membrane protein function result from changes in bilayer thickness per se. It remains unclear to what extent changes in intrinsic lipid curvature per se alter membrane protein function because experimental manipulations that alter the curvature, e.g., replacing phosphatidylcholine by phosphatidylethanolamine head groups, also alter other bilayer properties, such as bilayer thickness [18–21] and the ability to form hydrogen bonds [22,23]. Moreover, amphiphiles that cause positive or negative changes in intrinsic lipid curvature, e.g., Triton X-100 or capsaicin, have similar effects on the function of gramicidin and voltage-gated sodium channels [24], indicating that they alter bilayer properties other than curvature—e.g., lipid bilayer elasticity [14,25–28]—and that the (amphiphile-induced) curvature changes are less important determinants of channel function in these experiments.

To further explore the relative importance of curvature and other bilayer properties, such as elasticity, we explore how molecules that produce positive curvature (Triton X-100, TX100 and reduced Triton X-100, rTX100) and negative curvature changes (capsaicin, Cpsn) alter the function of alamethicin channels and relate the changes in alamethicin channel function to the changes in gramicidin channel function. These channels are regulated by maneuvers that alter intrinsic lipid curvature [21,29,30] in hydrocarbon-containing planar lipid bilayers where thickness changes are minimal [21,30,31], making them suitable for the present study.

The alamethicins and the linear gramicidins are channel-forming peptide antibiotics that are synthesized by nonribosomal peptide synthases (NRPs) [32]. As for most peptides synthesized by NRPs, the sequences have nongenetic amino acids: in the case of the gramicidins, D-amino acids; in the case of alamethicin, α-aminoisobutyric acid (Aib) and phenylalaninol (Pheol). The linear gramicidins are 15 amino acid peptides produced by the soil bacillus *Bacillus brevis*. They occur in a number of sequence variants; the predominant species, [Val^1]gramicidin A (or gA), has the sequence listed in Figure 1A. The alamethicins are 20 amino acid peptides produced by the soil fungus *Trichoderma viride*. As is the case for the linear gramicidins, alamethicin occurs in a number of sequence variants; the predominant species, alamethicin I (or Alm), has the sequence listed in Figure 1B.

gA and Alm channels have been used extensively to probe changes in lipid bilayer properties as sensed by bilayer-spanning channels; for reviews, see [8,33]. They complement each other because of the different channel structures and mechanisms of formation (Figure 1).

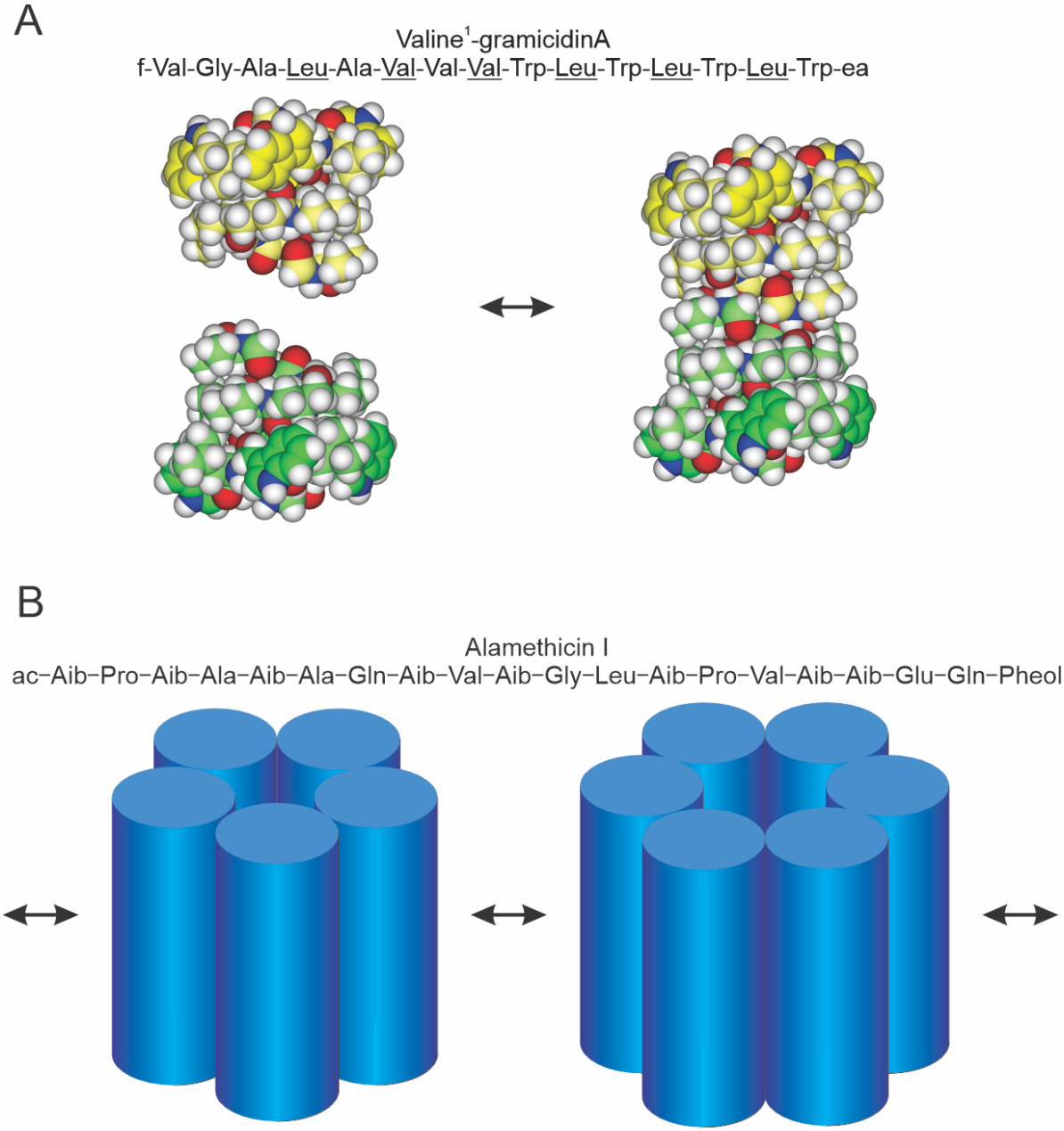

Figure 1. Schematic models of gramicidin and alamethicin channels. (**A**) Top: sequence of [Val[1]]gA [34], the major gramicidin species in naturally occurring mixture of peptides [35]; f is formyl, ea ethanolamine and the D-amino acids are underlined. Bottom: gramicidin channels form and disappear, as indicated by the arrows, by a transmembrane association/dissociation [36]. Left, atomic resolution structures of the $\beta^{6.3}$-helical monomers, the two subunits are depicted some distance apart; right, atomic resolution structure of the $\beta^{6.3}$-helical conducting dimer. The carbons in the two subunits are colored green and yellow, respectively, with the carbon atoms in the Trp side chains emphasized. Blue is nitrogen, red is oxygen and white is hydrogen. (**B**) Top: sequence of alamethicin I [37], the major species of alamethicin; ac is acetate, Aib α-isobutyric acid and Pheol phenylalcohol. Bottom: different interconverting oligomeric states, as indicated by the arrows, of the bilayer-spanning channel. The number of subunits may change by the association/dissociation of bilayer-spanning subunits or oligomers or by the accretion of subunits at the bilayer/solution interface that inserts into the bilayer [33,38].

gA channels (Figure 1A) form by the bimolecular association of two nonconducting subunits [39–43], one from each bilayer leaflet [36]; see [44] for a summary of the evidence. The channel structure, a $\beta^{6.3}$-helical dimer, is known from high-resolution solution nuclear magnetic resonance (NMR) studies on gA incorporated into sodium dodecyl sulfate micelles [45,46] and solid-state NMR studies on gA incorporated into oriented lipid bilayers [47,48]. Minor differences between the structures determined in solution NMR and solid-state NMR can be resolved using molecular dynamics simulations to allow for local motion and motional averaging [49].

Except for extreme changes in bilayer thickness [50–52] or curvature [53], the gramicidin channel structure is remarkably unaffected by changes in bilayer thickness [54,55]. The current transitions associated with channel formation and disappearance have a single predominant amplitude [56] that varies little with changes in bilayer thickness [27,57,58].

The channel's hydrophobic length is less than the bilayer hydrophobic thickness, meaning that channel formation leads to a local bilayer thinning [59–62]. The free energy difference of channel formation ($\Delta G_{tot}^{M\rightarrow D}$), thus, will include a contribution from the lipid bilayer ($\Delta G_{bil}^{M\rightarrow D}$), and the gA monomer↔dimer equilibrium will vary as a function of changes in lipid bilayer properties [8]. These gA channel characteristics make them useful as tools to probe changes in lipid bilayer properties, as sensed by bilayer-spanning proteins.

Less is known about Alm channels, which form voltage-dependent multi-state channels [63,64]; for reviews, see [33,38,65–68]. Alm was crystallized from organic solvents, and the structure was solved by X-ray crystallography [69], which revealed a predominantly α-helical structure. The structure of the bilayer-associated Alm is α-helical, as deduced from solid-state NMR [70] and oriented circular dichroism spectroscopy [71]. The orientation of the bilayer-associated Alm varies as a function of the Alm/lipid mole fraction [38,71,72]. At low Alm/lipid mole fractions (<1/100), where Alm is monomeric [70], the helical axis is parallel with the bilayer/solution interface; at high Alm/lipid mole fractions (>1/50), the helical axis is perpendicular to the bilayer/solution interface. The transition between these two states depends on the bilayer composition [38] and occurs at Alm/lipid ratios near the cooperative transition in the adsorption isotherm [73]. The switch between the parallel (adsorbed) and perpendicular (inserted) state can be understood in terms of a build-up of elastic curvature stress in the bilayer [74], as the bilayer thickness decreases with increasing Alm mole fraction until the mole fraction where the switch from the adsorbed to inserted state occurs [38].

Alm channels are barrel-stave assemblies of bilayer-spanning α-helices [75–77], as originally proposed by Bauman and Mueller [78] and Boheim [64], with multiple current levels. It is generally accepted that the different conductance states reflect different peptide stoichiometries. It remains unclear whether the different current levels represent transitions within a single multimeric barrel-stave channel with different Alm stoichiometries [64,78,79] or an array of closely packed parallel pores [80], where the different current levels reflect the association/dissociation of Alm monomers or nonconducting Alm aggregates. Neutron [81] and X-ray diffraction [76] experiments provide support for a well-defined water-filled pore with a 10° to 20° tilt relative to the bilayer normal as deduced by solid-state NMR [82]. Probing the pore diameter using polyethyleneglycols of different sizes [80] provides support for a multipore cluster. Both models are consistent with mechanoelectrical experiments [79], which show that the different conductance states differ in total area by ~1.2 nm^2—a number that can be decomposed into a contribution from the Alm monomer, ~0.8 nm^2 [83], and from the water-filled pore, ~0.4 nm^2, with the latter being similar to the area changes deduced from the measured current changes [84].

Both gA and Alm channels are sensitive to changes in bilayer properties. In the case of Alm channels, the higher current levels are stabilized by changes in phospholipid head groups and head group interactions that cause negative changes in intrinsic lipid curvature [29,33,85]. In the case of gA channels, the single-channel appearance rates and lifetimes (and, thus, the time-averaged channel surface densities and the channel activity) are reduced by changes in head group interactions that cause negative changes

in curvature [21,30]. Yet, the role of curvature in the regulation of gA channel function is complex because channel activity is increased by reversibly adsorbing amphiphiles that produce positive as well as negative changes in curvature [24,27]. These seemingly contradictory results arise because reversibly adsorbing amphiphiles for thermodynamic reasons [25,26] increases lipid bilayer elasticity [14,24–26,28,86–88].

A similar result was observed with voltage- and ligand-gated channels in biological membranes. Reversibly adsorbing amphiphiles inhibit voltage-gated sodium channels (Na_V) by causing a hyperpolarization shift in the steady-state channel availability curve [24,89] and causing the desensitization of the $GABA_A$ receptor [90]. In either case, amphiphiles that cause positive and negative changes in curvature cause similar changes in channel function, and, in the case of Na_V, the shift in inactivation is correlated with the changes in gA channel lifetime [14,24].

We, therefore, explored how the reversibly partitioning amphiphiles TX100, rTX100 and Cpsn alter the function of Alm channels and related the changes in the Alm channel function to the changes in gA channel lifetimes. We find that the amphiphile-induced changes in the Alm channel function (the distribution among the different current levels) are correlated to the changes in the gA channel function (single-channel lifetime). We conclude that changes in bilayer elasticity are more important than changes in curvature in terms of modulating Alm channel function, like what was found with gA channels.

2. Results

2.1. Amphiphiles Modulate Alm Channel Function

TX100, rTX100 and Cpsn are potent modifiers of Alm channel function. Figure 2 shows current traces obtained before and after the addition of Cpsn, TX100 or rTX100 to both sides of a bilayer (Alm was present on one side only; potentials are measured relative to the Alm-free solution). Amphiphiles may exert their effects by mechanisms that do not involve changes in bilayer mechanical properties, including changes in the interfacial dipole potential [91,92], and asymmetric addition of amphiphiles that alter the dipole and/or surface potential may exert their effects on Alm channel function by changes in the electric field within the membrane [93], a complication we strived to avoid with symmetric addition of the amphiphiles. Because we wished to focus on the amphiphiles' bilayer effects, all experiments were performed at a single membrane potential (150 mV).

The three amphiphiles increased the Alm channel activity (time-averaged number of conducting channels) and shifted the distribution among current levels toward higher current levels. The short time traces at the bottom of Figure 2 show that the different conduction levels in Alm channels do not vary in the presence of TX100, rTX100 and Cpsn. (The current levels observed in the absence of amphiphiles are summarized in Table S1; Table 1 summarizes information on the lack of amphiphile effects on the current levels). TX100 and rTX100 were equally effective in producing the change in Alm channel function; threefold higher concentrations of Cpsn were needed to observe changes comparable to those observed with TX100 and rTX100. Though the amphiphiles did not cause obvious changes in the baseline current, the bilayers were destabilized. In the absence of amphiphiles, we could record current traces for several minutes; in the presence of amphiphiles, we usually could record for no more than 2 min before the small membrane (patch) broke.

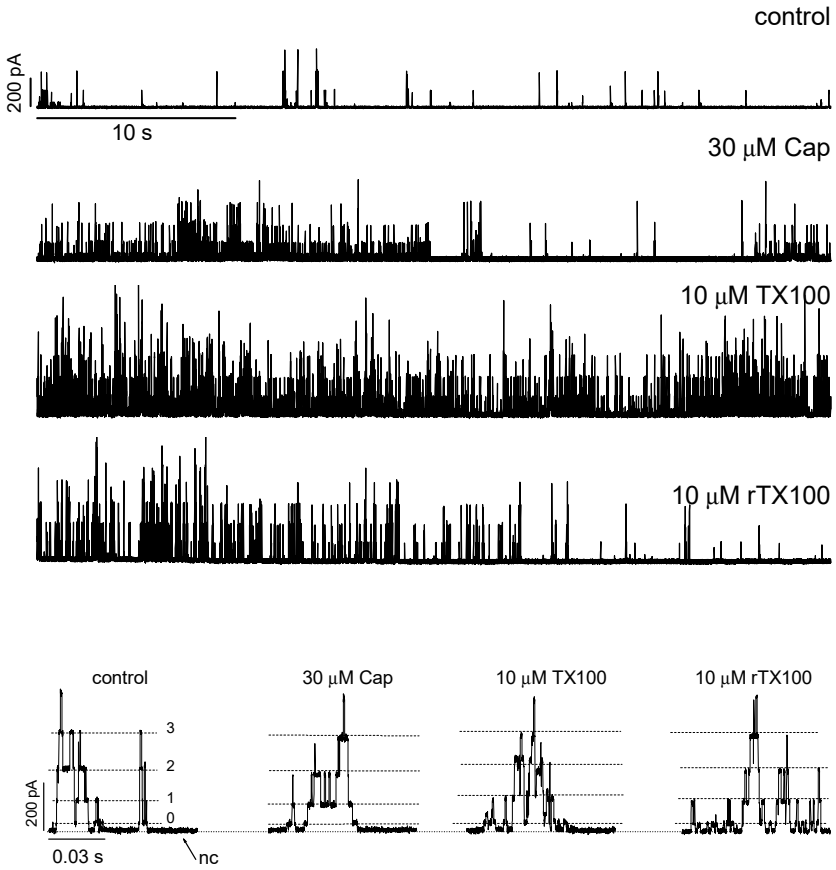

Figure 2. Amphiphile-induced changes in alamethicin channel activity. Cpsn, TX100 and rTX100 increase Alm channel activity. Top four records: 40 s recorded before the addition of amphiphile and after the addition of the indicated amphiphile (the control traces were similar for each amphiphile trace). The calibration bars in the top trace apply to all four traces. Bottom four traces show the effect of the amphiphiles at higher resolution; calibration bars in the control trace segment apply to all the trace segments. The stippled lines denote different current levels; they do not vary with amphiphile addition (Table 1) (DOPC, 1.0 M NaCl, pH 7.0, 150 mV).

Table 1. Alm channel current levels 0–3 in the absence and presence of TX100, rTX100 and Cpsn.

	Level 0 (pA)	**Level 1 (pA)**	**Level 2 (pA)**	**Level 3 (pA)**
DOPC	4.5 ± 0.2	18.0 ± 0.5	38.4 ± 0.8	61 ± 1
+30 μM Cpsn	4.4 ± 0.3	17.7 ± 0.8	37.8 ± 0.9	60 ± 1
+30 μM TX100	4.5 ± 0.1	18.6 ± 0.6	39.5 ± 0.3	60 ± 1
+30 μM rTX100	4.5 ± 0.2	16.7 ± 0.6	36.8 ± 0.8	59 ± 1

Each datum (Mean ± S.D.) is based on current amplitude histograms (all-points histograms, cf. Figure 3) from at least three independent experiments conducted on different days, with one to three measurements for each condition on a given day (1.0 M NaCl, 10 mM HEPES (pH 7), 150 mV).

Alm channels occur as bursts of activity (Figure 2), and the time spent in the different Alm channel conducting states, as well as the time when no Alm channel activity could be observed, was determined from all-point histograms [94] based on 1–3 min current traces (Figure 3), which showed that the amphiphiles increased the channel activity and shifted the distribution of current levels toward higher levels.

For each histogram, the peaks representing the no-channel state (current level *nc*) and the different conducting states (current levels 0, 1, 2, 3 . . . *n*) were identified and fitted by Gaussian fits, and the area under each peak was calculated to determine the time spent

in that channel state. We sometimes observed multiple Alm channels at the same time, which complicated the assignment of the peaks in the histograms to channel states. We tried to exclude such multiple channel records from the analysis, which may lead to an underestimation of the amphiphile-induced changes in Alm channel activity. This was not always possible after the addition of Cpsn, TX100 or rTX100, which increased channel activity. In this case, we assigned the peaks in the all-points histograms to the underlying current levels. When that was not possible, we did not use the data.

The reported results are based on at least 60 s of continuous recording to minimize the errors introduced by temporal changes in channel activity. On a given day, it was usually possible to obtain three recordings in three different small membranes; each data point is based on at least recordings obtained on at least three different days.

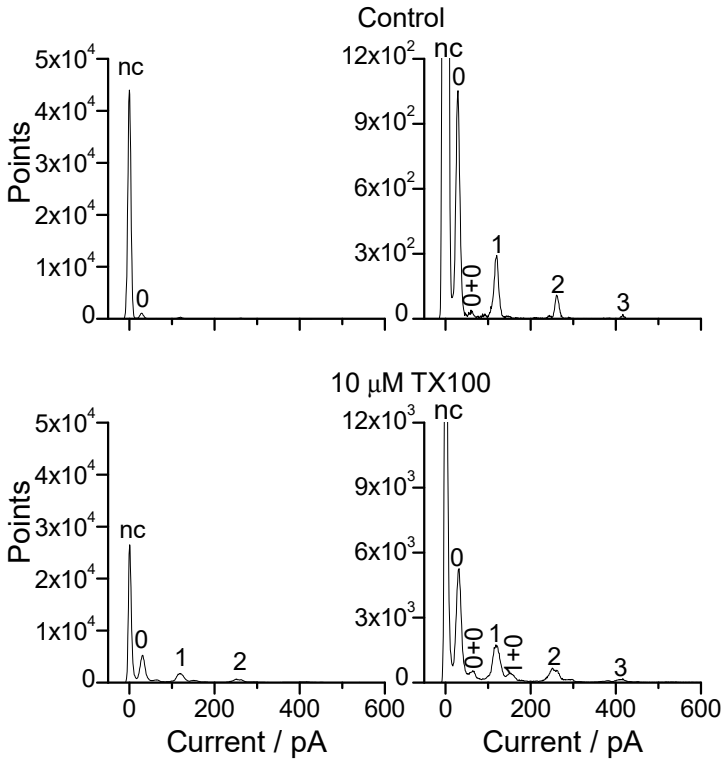

Figure 3. Current level (all-point) histograms showing the effects of TX100 on Alm channel function, results from one experiment. Top: results from a 40 s recording before the addition of TX100. Bottom: results from a 40 s recording in the same membrane a few min after the addition of 10 μM TX100. The right panels show the same results as the left but at an expanded scale for the ordinate. nc denotes the no-channel current level; the plots were aligned such that the nc peak is centered at 0 pA. The numbers over the peaks denote the identity of the channel state; two numbers indicate that the peak results from the superposition of two different channels (DOPC, 1.0 M NaCl, pH 7.0, 150 mV).

To facilitate comparison of different experiments, each histogram was adjusted (by a few pA) such that the peak representing the baseline was at 0 pA. In both the absence and presence of TX100, each current level is indicated by a well-defined peak, which does not vary as the amphiphile is added (similar results were found with rTX100 and Cpsn). Following Hanke and Boheim [84], the current levels are denoted as 0, 1, 2, 3, etc., with the highest level we observe in the presence of the amphiphiles being 7. Table 1 summarizes our results for TX100, rTX100 and Cpsn. The amphiphiles do not shift the current levels, indicating that the amphiphiles produce minimal changes in the channel structure associated with the different current levels. This result is in general agreement with a barrel-stave structure for the conducting channels [76,81].

In some cases, there were small, secondary peaks between the main current levels (e.g., Figure 3, histograms in right column). These peaks represent the summed current through

two different channels, e.g., level 0 + level 0, denoted as (0 + 0); level 1 + level 0, denoted as (1 + 0). Though we strived to use records with only single channels, these secondary peaks often occurred after amphiphile addition because the amphiphiles increased the time-averaged number of conducting channels; they were incorporated into the data analysis and final results in case we could unambiguously assign the peaks to different current level combinations. If that was not possible, the results were not used.

The Alm channel activity was quantified as the ratio of time spent in any conducting level relative to the *nc* level (R_{Alm}):

$$R_{\mathrm{Alm}} = \left(\sum_{\mathrm{i}=0}^{\mathrm{n}} A_{\mathrm{i}}\right) / A_{\mathrm{nc}}; \tag{2}$$

where A_{nc} denotes the area under the peak representing the baseline current (the no-channel state) and A_{i} the area under the peak representing current level i (i = 0, 1, 2, 3, . . ., n, using the nomenclature of [84], where n + 1 is the maximal number of current levels observed in the experiment).

The amphiphile-induced changes in Alm channel activity could, thus, be quantified as

$$\frac{R_{\mathrm{Alm}}^{\mathrm{AM}}}{R_{\mathrm{Alm}}^{\mathrm{cntl}}} = \frac{\left(\sum_{\mathrm{i}=0}^{\mathrm{n}'} A_{\mathrm{i}}^{\mathrm{AM}}\right) / A_{\mathrm{nc}}^{\mathrm{AM}}}{\left(\sum_{\mathrm{i}=0}^{\mathrm{n}} A_{\mathrm{i}}^{\mathrm{cntl}}\right) / A_{\mathrm{nc}}^{\mathrm{cntl}}}, \tag{3}$$

where the superscripts AM and cntl denote results obtained in the presence (AM) or absence (cntl) of amphiphile, and n + 1 and n' + 1 denote the maximum number of current levels (including level 0) observed in the absence and presence of the amphiphile.

The overall channel activity, evaluated as R_{Alm} (Equation (2)), is stationary over the duration of the recordings. Figure 4 shows the variation in R_{Alm} evaluated over 10 s time intervals as a function of time.

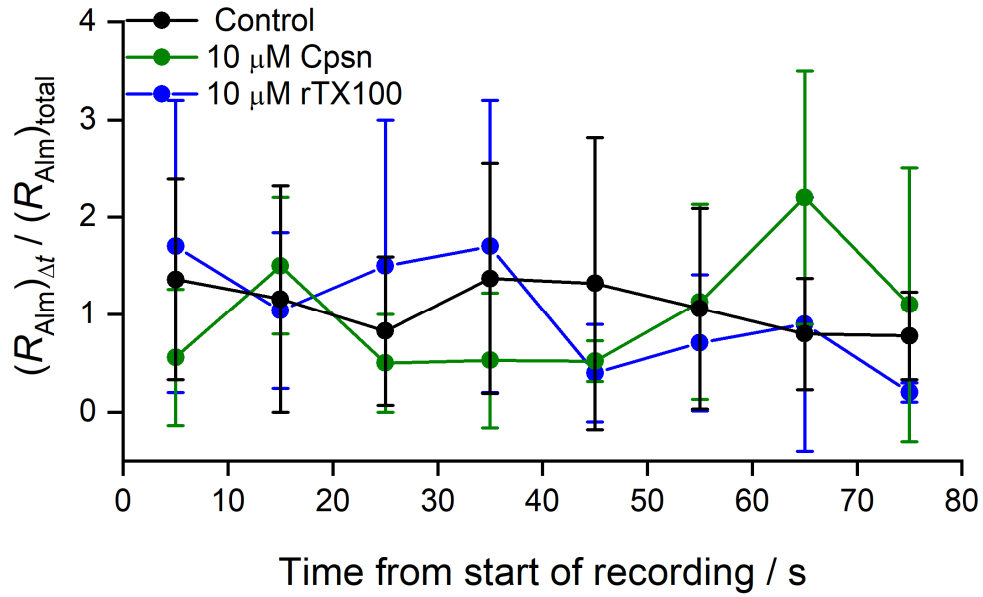

Figure 4. The variability of Alm channel activity as a function of time in the absence or presence of amphiphile. The ordinate denotes the channel activity, the time the channels reside in any conducting state relative to the no-channel state (R_{Alm}, Equation (2)) over a 10 s time interval, normalized to the average activity over the total 80 s recording time. Mean ± S.D. based on at least three independent experiments at each condition (DOPC, 1.0 M NaCl, pH 7.0, 150 mV).

The Alm channel activity varied over time (as also evident in the traces in Figure 2), but there was no systematic trend.

The probability of a channel being in current level k (W_k) was estimated as follows:

$$W_k = \frac{A_k}{A_{nc} + \sum_{i=0}^{n} A_i} \tag{4}$$

where A_{nc} and A_i i (i = 0, 1, 2, 3, …, n; n + 1 is the maximal number of current levels observed in the experiment) denote the areas under the peak representing current level, which is proportional to the time spent in each current level. (The nominator in Equation (4) is the total area under the histogram, which is proportional to the recording time for that experiment).

The time spent in current level k, relative to the no-channel state (nc), A_k/A_{nc}, provides a measure of $\Delta G^{nc\to k}$, the free energy difference current level k relative to the nc state:

$$\Delta G^{nc\to k} = k_B T \cdot \ln\{W_k/W_{nc}\} = k_B T \cdot \ln\{A_k/A_{nc}\}, \tag{5}$$

where T is the temperature in kelvin and k_B Boltzmann's constant. The amphiphile-induced changes in channel function (the ratio of the probabilities of being in current level k relative to the nc level) can then be expressed as follows:

$$\frac{A_k^{AM}/A_{nc}^{AM}}{A_k^{cntl}/A_{nc}^{cntl}} = \exp\left\{-\frac{\Delta G^{nc\to k,AM} - \Delta G^{nc\to k,cntl}}{k_B T}\right\} = \exp\left\{-\frac{\Delta\Delta G^{nc\to k}}{k_B T}\right\}. \tag{6}$$

The distribution among current levels, e.g., between levels j and k, was determined from the amphiphile-induced changes in A_k/A_j; it was, thus, possible to obtain estimates for the free energy differences between the two channel states:

$$\frac{A_k^{AM}/A_j^{AM}}{A_k^{cntl}/A_j^{cntl}} = \exp\left\{-\frac{\Delta G^{j\to k,AM} - \Delta G^{j\to k,cntl}}{k_B T}\right\} = \exp\left\{-\frac{\Delta\Delta G^{j\to k}}{k_B T}\right\}. \tag{7}$$

The amphiphile-induced changes in Alm channel activity are summarized in Figures 5–7. Figure 5 shows the changes in overall channel activity, R_{Alm}, which increases as an approximately linear function of [AM]. Figure 6 shows the changes in the distribution of current levels relative to the no-channel level (cf. Equation (5)), where the results are plotted as $\ln\{(A_i^{AM}/A_{nc}^{AM})/(A_i^{cntl}/A_{nc}^{cntl})\}$ (=$-\Delta\Delta G^{nc\to i}/k_B T$) vs. [AM]. Figure 7 shows the changes in the stability of current levels 2 and 3 relative to level 1 (cf. Equation (7)). The amphiphile-induced stabilization is more pronounced for the higher current levels (Figures 6 and 7), with a tendency to level off at higher [AM].

The amphiphile-induced changes in Alm channel function, with amphiphiles that promote negative and positive curvatures having similar effects, were surprising in light of the results of Keller et al. [29] and Bezrukov et al. [85], who showed that changes in phospholipid head group size [29] or charge [85] that promote negative curvatures stabilize the higher Alm channel current levels. Given the slightly different membrane compositions, Keller et al. [29] and Bezrukov et al. [85] used *n*-hexadecane, and we used *n*-decane, so we reexamined whether this relation also holds in our system. It did, as shown in Figures S1–S3 in Supplemental Information, confirming that Alm channels are, indeed, regulated by changes in curvature. We conclude that changes in bilayer properties other than curvature are also important for Alm channel function, which we explored using the gA channels as probes.

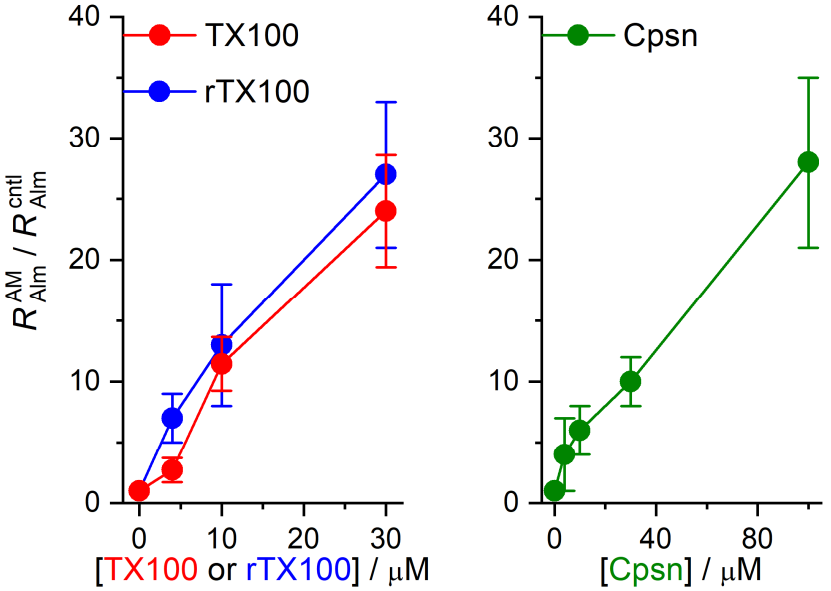

Figure 5. Effect of amphiphiles (TX100, rTX100 or Cpsn) on Alm channel activity. The ordinate displays the channel activity (Equation (2)) in the presence of amphiphile divided by the activity in the absence of amphiphile ($R^{AM}_{Alm}/R^{cntl}_{Alm}$, cf. Equation (3)). Mean ± S.D. based on at least three independent experiments, with one to three measurements, at each condition (DOPC, 1.0 M NaCl, pH 7.0, 150 mV).

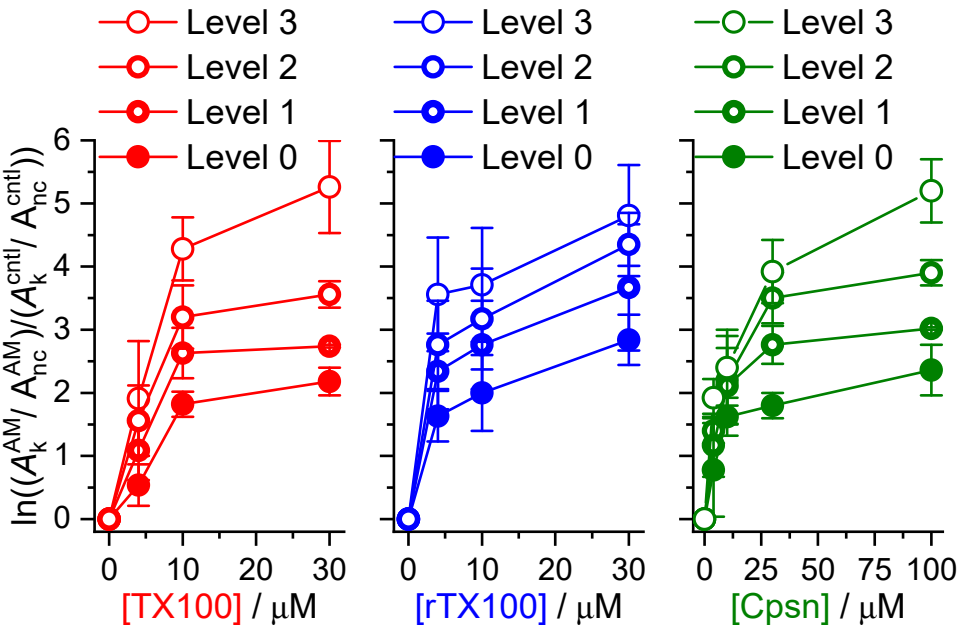

Figure 6. Effect of TX100, rTX100 or Cpsn on the distribution of Alm channel current levels relative to the nc level. The ordinate depicts the changes in $\ln\left\{\left(A^{AM}_k/A^{AM}_{nc}\right)/\left(A^{cntl}_k/A^{cntl}_{nc}\right)\right\}$, k = 0, 1, 2, 3, cf. Equation (6). Mean ± S.D. based on at least three independent experiments, each with one to three measurements, at each condition (DOPC, 1.0 M NaCl, pH 7.0, 150 mV).

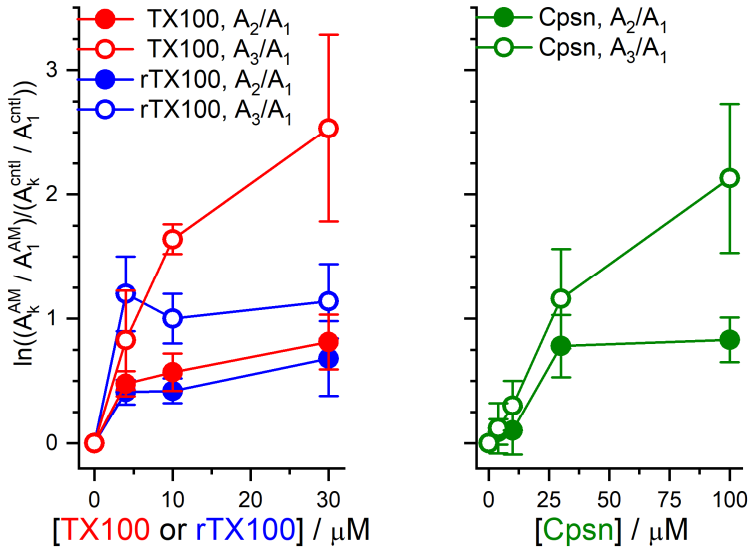

Figure 7. Effect of TX100, rTX100 or Cpsn on the distribution of time spent in different Alm current levels relative to the time spent in level 1. The ordinate shows $(\ln\left\{(A_k^{AM}/A_1^{AM}/(A_k^{cntl}/A_1^{cntl})\right\}$, k = 2, 3cf. Equation (7)). Left, results for TX100 and rTX100. Right, results for Cpsn. Mean ± S.D. based on at least three independent experiments, each with one to three measurements, at each condition (DOPC, 1.0 M NaCl, pH 7.0, 150 mV).

2.2. Amphiphile Modulation of gA Channel Stability

TX100, rTX100 and Cpsn are potent modifiers of gA channel function [24,89,95]. Figure 8 shows single-channel current traces before and after the addition of 10 μM TX100 or 30 μM Cpsn to the aqueous phases bathing a DOPC bilayer doped with gA^-(13) and AgA(15).

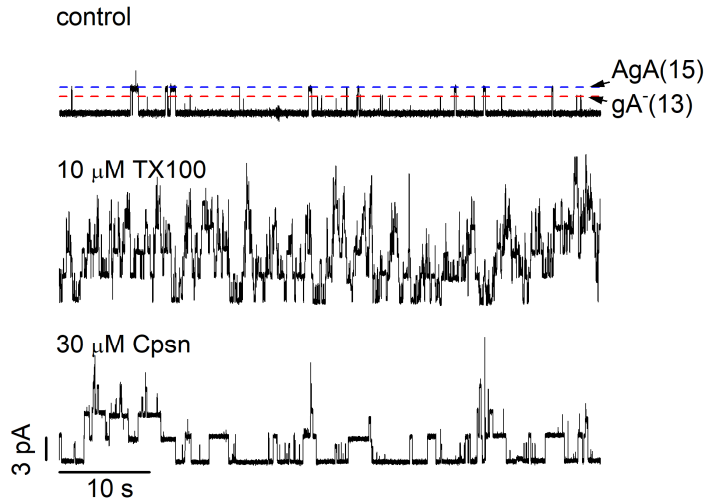

Figure 8. TX100 and Cpsn produce similar increases in gA channel activity. The three traces denote 60 s current traces recorded in the absence or presence of either 10 μM TX100 or 30 μM Cpsn (the control trace is from the TX100 experiment; similar single-channel activity was observed in the control trace for Cpsn). The experiments were performed using two different gA analogs, AgA(15) and gA^-(13), which were added together to both sides of the bilayer. AgA(15) and gA^-(13) channels can be distinguished by their current transition amplitudes (indicated by the horizontal dashed lines in the control current trace: blue for AgA(15) channels; red for gA^-(13) channels). The calibration bars in the bottom trace apply to all traces (DOPC, 1.0 M NaCl, pH 7.0, 200 mV).

These experiments were analyzed by constructing single-channel current transition amplitude histograms [96], where the current transitions associated with each channel type appear as a single peak, which allows for determining the single-channel lifetimes (τ) for each channel type [13] by matching channel appearances to disappearances, e.g., [97]; lifetime histograms were constructed and transformed into survivor distributions. The average channel lifetimes ($\tau = 1/k_{-1}$, where k_{-1} is the dissociation rate constant for the bilayer-spanning, conducting channel, D) were determined by fitting a single exponential distribution, $N(t)/N(0) = \exp\{-t/\tau\}$, where $N(t)$ denotes the number of channels with a lifetime longer than time t, to the normalized survivor distributions.

The dimeric gA channels (D) form by the transbilayer association of two non-conducting monomers (M):

$$2\,\mathrm{M} \underset{k_{-1}}{\overset{k_1}{\rightleftarrows}} \mathrm{D},$$

where k_1 is the rate constant for channel dimerization and k_{-1} the rate constant for channel dissociation (and $\tau = 1/k_{-1}$). To quantify the amphiphiles' effect on the channel appearance rate ($f = k_1 \cdot [\mathrm{M}]^2$, where [M] is the gA monomer concentration), we determined the channel appearance rates based on three (5–10 min) recordings obtained before and 10–20 min after addition of TX100, rTX100 or Cpsn (some results for Cpsn are from Ref. [24]). Only bilayers that did not break during amphiphile addition were used for the analysis.

The relative changes in the time-averaged channel "concentrations" were determined as the ratio of the product of the channel appearance rate and lifetime—measured before and after the amphiphile addition [98]:

$$\frac{[\mathrm{D}]^{\mathrm{AM}}}{[\mathrm{D}]^{\mathrm{cntl}}} = \frac{f^{\mathrm{AM}} \cdot \tau^{\mathrm{AM}}}{f^{\mathrm{cntl}} \cdot \tau^{\mathrm{cntl}}} = \frac{k_1^{\mathrm{AM}} \cdot [\mathrm{M}]^2 / k_{-1}^{\mathrm{AM}}}{k_1^{\mathrm{cntl}} \cdot [\mathrm{M}]^2 / k_{-1}^{\mathrm{AM}}} = \frac{K_{\mathrm{D}}^{\mathrm{AM}}}{K_{\mathrm{D}}^{\mathrm{cntl}}}, \tag{8}$$

where the second and the third equalities hold in the limit [M]>>[D], such that $[\mathrm{M}]^{\mathrm{AM}} \approx [\mathrm{M}]^{\mathrm{cntl}}$. Changes in the free energy of gramicidin channel formation, $\Delta\Delta G^0_{\mathrm{tot}}$, which should be equal to the AM-induced change in $\Delta G^0_{\mathrm{def}}$, were evaluated as follows:

$$\Delta\Delta G^0_{\mathrm{tot}} \; (\approx \Delta\Delta G^0_{\mathrm{bil}}) = -k_{\mathrm{B}}T \cdot \ln\left\{\frac{K_{\mathrm{D}}^{\mathrm{AM}}}{K_{\mathrm{D}}^{\mathrm{cntl}}}\right\} = -k_{\mathrm{B}}T \cdot \ln\left\{\frac{f^{\mathrm{AM}} \cdot \tau^{\mathrm{AM}}}{f^{\mathrm{cntl}} \cdot \tau^{\mathrm{cntl}}}\right\}. \tag{9}$$

The final results for a given experimental condition are reported as the mean ± standard deviation (SD) based on at least three independent measurements.

Though TX100 and Cpsn cause opposite changes in curvature [24], they both increase the channel appearance frequencies (f), lifetimes (τ) and, thus, the time-averaged channel densities in the bilayer ($f \cdot \tau$), and they reduce the bilayer deformation energy $\Delta\Delta G^{\mathrm{M}\to\mathrm{D}}_{\mathrm{bilayer}}$, with the larger effects on the shorter $\mathrm{gA}^-(13)$ channels. Figure 9 shows results for TX100, rTX100 and Cpsn; Figure 10 (below) shows how all three amphiphiles increase gA channel lifetimes.

As was the case for Alm channels, one needs about three-fold higher [Cpsn] than [TX100] or [rTX100] to observe comparable changes in channel function, f and τ.

The results in Figure 9 can be interpreted further using the theory of elastic bilayer deformations, in which the bilayer deformation energy associated with the hydrophobic adaptation of the bilayer to an embedded protein is expressed as a biquadratic function in the channel-bilayer hydrophobic mismatch ($d_0 - l$) and intrinsic lipid curvature (c_0), [15], Equation (17):

$$\Delta G_{\mathrm{def}} = H_{\mathrm{B}} \cdot (d_0 - l)^2 + H_{\mathrm{X}} \cdot (d_0 - l) \cdot c_0 - H_{\mathrm{C}} \cdot c_0^2 \tag{10}$$

where H_{B}, H_{X} and H_{C} are elastic coefficients that are functions of bilayer thickness, elastic moduli and channel radius (and include contributions from the energetic cost of redistributing the different components in a multi-component membrane, including the redistribution of the *n*-decane in our planar bilayer experiments). Equation (10) was derived from

the theory of elastic bilayer deformations [15,99], and estimates for H_B, H_X and H_C can be obtained from Equation (17) and Table 4 in reference [15]: $H_B \approx 350$ kJ/(mol·nm^2), $H_X \approx -290$ kJ/mol and $H_C \approx -40$ (kJ/mol)·nm^2. The biquadratic form, however, applies more generally [6,14]. gA channels function, for example, is regulated by lipid bilayer thickness [58,59,100] and intrinsic lipid curvature [21,30], meaning that ΔG^0_{def} can be expressed as a function of $(d_0 - l)$, c_0 and maybe other terms. Using a Taylor expansion in $(l - d_0)$ and c_0, ΔG^0_{def} becomes [14]:

$$\begin{aligned}\Delta G^0_{def}(d_0 - l, c_0) \quad &= \Delta G^0_{def}(0,0) + \frac{\partial(\Delta G^0_{def})}{\partial(d_0 - l)} \cdot (d_0 - l) + \frac{\partial(\Delta G^0_{def})}{\partial c_0} \cdot c_0 + \\ &+ \frac{1}{2}\frac{\partial^2(\Delta G^0_{def})}{\partial(d_0 - l)^2} \cdot (d_0 - l)^2 + \frac{\partial^2(\Delta G^0_{def})}{\partial(d_0 - l)\partial c_0} \cdot (d_0 - l) \cdot c_0 + \frac{1}{2} \cdot \frac{\partial^2(\Delta G^0_{def})}{\partial c_0^2} \cdot c_0^2 + \ldots,\end{aligned} \tag{11}$$

where the first-order terms will be zero when the bilayer can be approximated as an elastic body. (The deformation energy for small decreases in $(d_0 - l)$ should equal that for small increases, with a similar argument holding for c_0). The biquadratic form of ΔG^0_{def} in Equation (10), thus, should be valid quite generally with the following:

$$H_B = \frac{1}{2} \cdot \frac{\partial^2(\Delta G^0_{def})}{\partial(d_0 - l)^2}, \; H_X = \frac{\partial^2(\Delta G^0_{def})}{\partial(d_0 - l)\partial c_0}, \text{ and } H_C = -\frac{1}{2} \cdot \frac{\partial^2(\Delta G^0_{def})}{\partial c_0^2}. \tag{12}$$

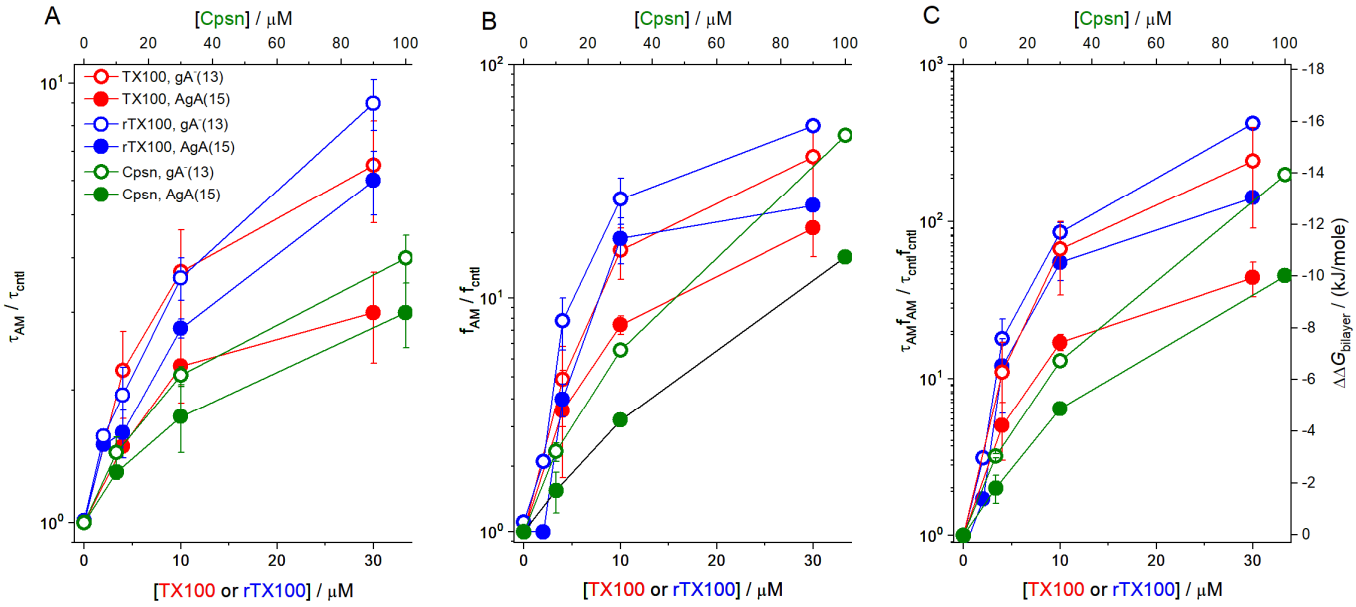

Figure 9. Effect of TX100, rTX100 and Cpsn on the lifetimes, appearance rates, channel activities and the change in the free energies of formation (Equation (9)) of AgA(15) and gA$^-$(13) channels. (Panel (**A**)) shows results for τ_{AM}/τ_{cntl}; (panel (**B**)) shows results for f_{AM}/f_{cntl}; (panel (**C**)) shows results for $\tau_{AM}{\cdot}f_{AM}/\tau_{cntl}{\cdot}f_{cntl}$. To facilitate comparison of the results for the 13-residue and 15-residue channels, the results are displayed using logarithmic y axes. In the control experiments for TX100, τ_{15} and τ_{13} were 160 ± 13 ms and 11.6 ± 1.4 ms, respectively; in the rTX100 experiments, τ_{15} and τ_{13} were 131 ± 7 ms and 11.0 ± 0.4 ms, respectively; in the Cpsn experiments, τ_{15} and τ_{13} were 206 ± 14 ms and 15.5 ± 0.2 ms, respectively. Filled symbols—results for AgA(15) channels; open symbols—results for gA$^-$(13) channels. Mean ± S.D. based on at least three independent experiments, each with three or more measurements, at each condition (DOPC, 1.0 M NaCl, pH 7.0, 200 mV).

In multi-component bilayers, the derivatives in Equations (11) and (12) include contributions from redistribution of bilayer components, whether it be lipids or hydrocarbon, meaning that Equation (10) should apply also for hydrocarbon-containing lipid bilayers, which can be approximated as elastic bodies [101–104]. The bilayer contribu-

tion to the gA channel monomer↔dimer equilibrium, $\Delta G_{bil}^{M\to D} = \Delta G_{def}^{D} - 2 \cdot \Delta G_{def}^{M}$, can, thus, be expressed as $\Delta G_{bil}^{M\to D} = H_B \cdot (d_0 - l)^2 + H_X \cdot (d_0 - l) \cdot c_0$, where we assume that $\Delta G_{def}^{M} = H_C \cdot c_0^2$.

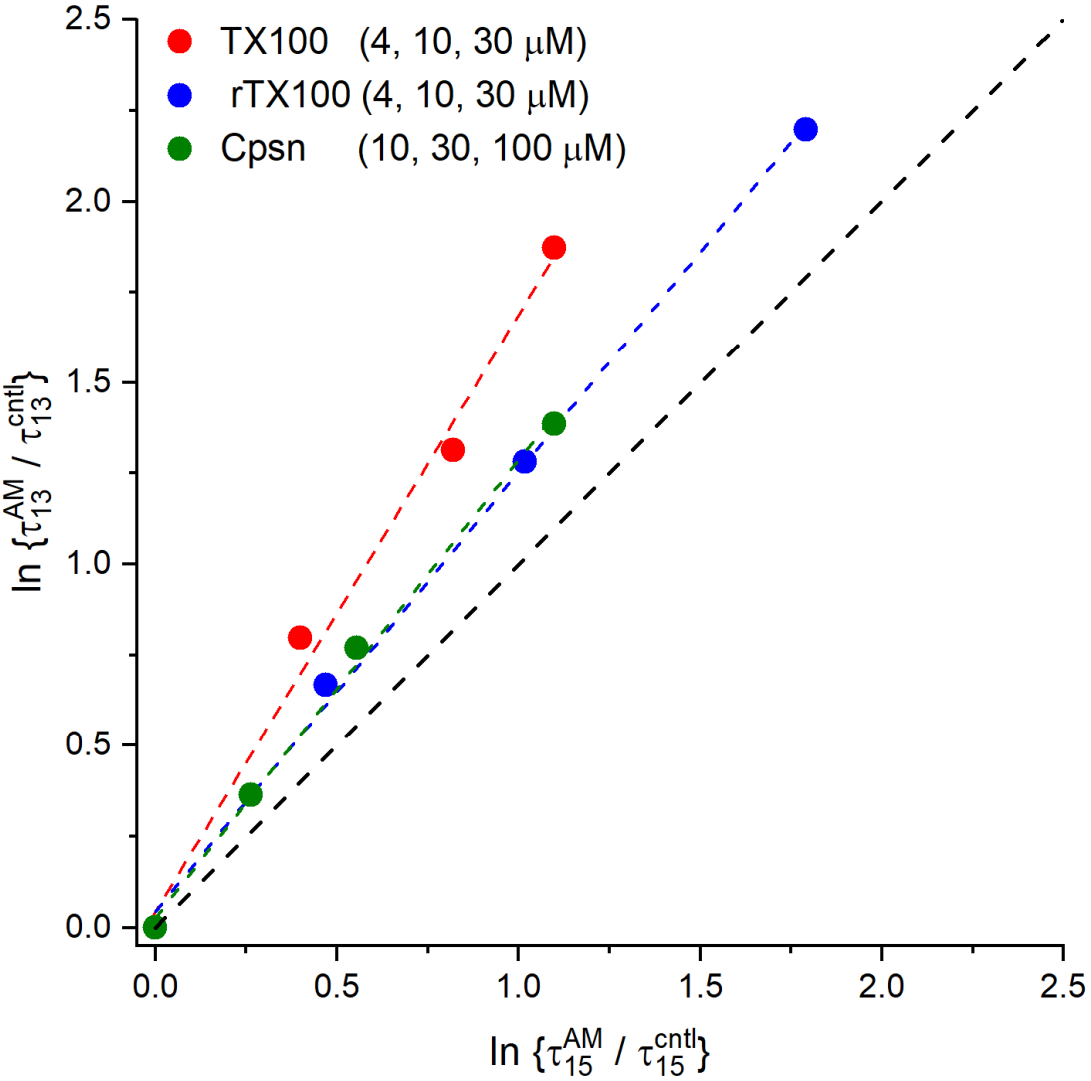

Figure 10. Amphiphiles produce larger relative changes in the lifetimes of $gA^{-}(13)$ channels, $\ln\left\{\tau_{13}^{AM}/\ \tau_{13}^{cntl}\right\}$, as compared to AgA(15) channels, $\ln\left\{\tau_{15}^{AM}/\ \tau_{15}^{cntl}\right\}$, based on results in Figure 9. The red, blue and green dashed lines denote linear fits to the result for TX100, rTX100 and Cpsn, respectively. For TX100, the slope was 1.64 ± 0.11, r^2 = 0.986 (90% confidence interval for the slope, 1.29–1.99); for rTX100, the slope was 1.21 ± 0.04, r^2 = 0.997 (90% confidence interval for the slope, 1.09–1.33); for Cpsn, the slope was 1.26 ± 0.05, r^2 = 0.995 (90% confidence interval for the slope, 1.10–1.42). The black interrupted line has a slope of 1. (DOPC, 1.0 M NaCl, pH 7.0, 200 mV).

The bilayer responds to the deformation by imposing a disjoining force (F_{dis}) on the channel [6,8]:

$$F_{dis} = -\frac{\partial(\Delta G_{def}^{0})}{\partial(d_0 - l)} = -2 \cdot H_B \cdot (d_0 - l) - H_X \cdot c_0, \quad (13)$$

and changes in F_{dis}—due, for example, to the adsorption of amphiphiles at the bilayer/solution interface—will be observable as changes in τ [8]:

$$\frac{\tau_{AM}}{\tau_{cntl}} = \exp\left\{-\frac{\left(F_{dis}^{AM} - F_{dis}^{cntl}\right) \cdot \delta}{k_B T}\right\}, \quad (14)$$

where δ denotes the distance the two subunits move apart to reach the transition state for channel dissociation [60,100]. The lifetime changes, with the larger changes for the shorter gA$^-$(13) channels with the larger hydrophobic mismatch, thus show that the amphiphiles alter the hydrophobic mismatch-dependent contribution to F_{dis}, the $2 \cdot H_B \cdot (d_0 - l)$ term. The lipid bilayer thickness does not change [21,24,31], meaning that $d_0 - l$ is invariant, and we conclude that the amphiphiles alter H_B or the bilayer elasticity. The arguments can be strengthened by combining the gA$^-$(13) and AgA(15) results, in which case Equation (14) becomes [8,14,21] the following:

$$\frac{\tau_{15}^{cntl} \cdot \tau_{13}^{AM}}{\tau_{15}^{AM} \cdot \tau_{13}^{cntl}} = \exp\left\{\frac{2 \cdot (H_B^{AM} - H_B^{cntl}) \cdot \delta \cdot (l_{13} - l_{15})}{k_B T}\right\}, \quad (15)$$

or

$$\ln\left\{\tau_{13}^{AM}/\tau_{13}^{cntl}\right\} = \ln\left\{\tau_{15}^{AM}/\tau_{15}^{cntl}\right\} + \frac{2 \cdot (H_B^{AM} - H_B^{cntl}) \cdot \delta \cdot (l_{13} - l_{15})}{k_B T}, \quad (16)$$

leading to

$$\frac{\tau_{13}^{amp}}{\tau_{13}^{cntl}} = \frac{\tau_{15}^{amp}}{\tau_{15}^{cntl}} \Rightarrow H_B^{amp} = H_B^{cntl}, \quad (17)$$

which holds irrespective of whether the amphiphiles (or changes in head group composition) alter lipid bilayer thickness.

We, therefore, examined the relationship between amphiphile-induced changes in $\tau_{13}^{AM}/\tau_{13}^{AM}$ and $\tau_{15}^{AM}/\tau_{15}^{AM}$, as shown in Figure 10.

As expected from previous studies [14,87,88,105], the amphiphiles produce greater changes in $\tau_{13}^{AM}/\tau_{13}^{cntl}$ than in $\tau_{15}^{AM}/\tau_{15}^{cntl}$, meaning that they increase bilayer elasticity.

The results in Figures 9 and 10 show that amphiphile-induced changes in intrinsic monolayer curvature do not predict the changes in channel lifetime. This does not mean that intrinsic lipid curvature is not important. As previously shown, increasing the mole fraction of DOPE in DOPC/DOPE bilayers, which causes a negative change in c_0 [29], leads to the same relative changes in the lifetimes of the shorter gA$^-$(13) and the longer AgA(15) channels, Figure S4 in the Supplemental Information and [21], meaning they do not alter bilayer elasticity (Equation (17)).

2.3. Comparison of Amphiphile Effects on Alm and gA Channel Function

Alm and gA channels have different structures/organization (Figure 1) and would, therefore, be expected to respond differently to changes in lipid bilayer properties. Yet, if the amphiphile-induced changes in channel function reflect general changes in bilayer properties, the changes in Alm and gA channel function should be related. That is the case (Figure 11).

Figure 11A shows how the overall Alm channel activity, $\ln\{R_{Alm}^{AM}/R_{Alm}^{cntl}\}$, varies as a function of $\ln\{\tau_{15}^{AM}/\tau_{15}^{cntl}\}$, which is proportional to ΔF_{dis}, the amphiphile-induced change in the disjoining force the bilayer imposes on the gA channels. Figure 11B shows how $\log\{(A_2^{AM}/A_1^{AM})/(A_2^{cntl}/A_1^{cntl})\}$, which is proportional to the change in the free energy between current levels 1 and 2 (cf. Equation (7)), varies as a function of $\ln\{\tau_{15}^{AM}/\tau_{15}^{cntl}\}$. Irrespective of the amphiphile-induced changes in curvature, the Alm channel activity and the relative stabilization of the higher current levels increase as the bilayer elasticity increases. The approximate linear relations between the changes in Alm and gA channel function show that both channels are regulated by changes in bilayer elasticity.

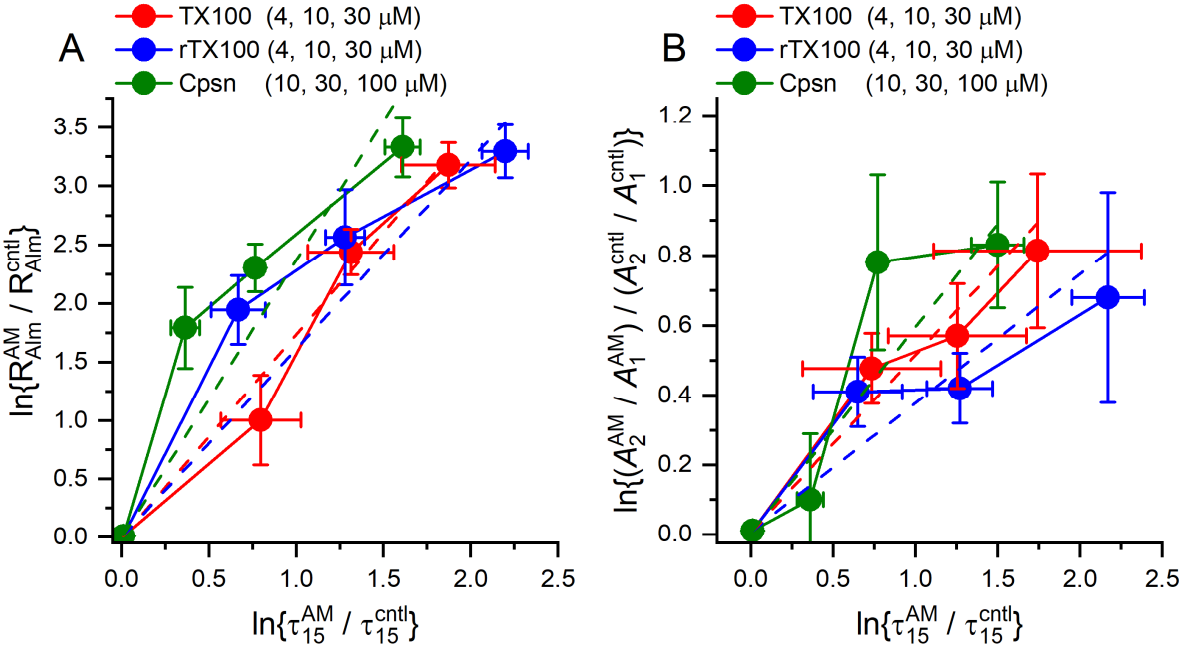

Figure 11. Amphiphile-induced changes in Alm function as functions of the changes in AgA(15) channel lifetimes. (**A**): Effect of TX100 (4, 10, 30 μM), rTX100 (4, 10, 30 μM) or Cpsn (10, 30, 100 μM) on Alm channel activity, expressed as $\ln\left\{R_{Alm}^{AM}/R_{Alm}^{cntl}\right\}$, cf. Equation (3), as functions of the corresponding changes in $\ln\left\{\tau_{15}^{AM}/\tau_{15}^{cntl}\right\}$. Based on results in Figures 5, 7 and 9. The red, blue and green dashed lines denote linear fits to the results, including 0 μM, for TX100, rTX100 and Cpsn, respectively. For TX100, the slope was 1.74, ± 0.08; r^2 = 0.994 (90% confidence interval for the slope, 1.15–3.60); for rTX100, the slope was 1.61 ± 0.22, r^2 = 0.940 (90% confidence interval for the slope, 0.89–2.33); for Cpsn, the slope was 2.37 ± 0.40, r^2 = 0.920 (90% confidence interval for the slope, 1.15–3.60) (DOPC, 1.0 M NaCl, pH 7.0). (**B**): Effect of TX100, rTX100 or Cpsn on the distribution between Alm current level 1 and 2, expressed as $\ln\left\{(A_2^{AM}/A_1^{AM})/(A_2^{cntl}/A_1^{cntl})\right\}$, cf. Equation (7), as functions of the corresponding changes in $\ln\left\{\tau_{15}^{AM}/\tau_{15}^{cntl}\right\}$. The dashed lines denote linear fits to the results, including 0 μM. For TX100, the slope was 0.51 ± 0.06, r^2 = 0.959 (90% confidence interval for the slope, 0.33–0.70); for rTX100, the slope was 0.37 ± 0.08, r^2 = 0872 (90% confidence interval for the slope, 0.13–0.61); for Cpsn, the slope was 0.59 ± 0.12, r^2 = 0.920 (90% confidence interval for the slope, 0.24–0.95) (DOPC, 1.0 M NaCl, pH 7.0).

3. Discussion

Our results extend previous studies on the bilayer regulation of Alm channels [29,85] and gA channels [21,30], which showed that the distribution of current levels in Alm channels and the stability of gA channels are regulated by changes in intrinsic lipid curvature associated with changes in phospholipid head group composition that produce changes in intrinsic curvature, whether changes in head group bulk or electrostatic repulsion among the head groups. Positive changes in curvature promote the formation of gA channels but destabilize the high-conductance states in Alm channels; negative changes in curvature changes destabilize gA channels but promote the high-conductance states in Alm channels.

Changes in curvature, however, are not the only membrane property that is important for Alm and gA channel function. The changes produced by TX100, rTX100 and Cpsn, reversibly partitioning amphiphiles that produce positive (TX100 and rTX100) and negative (Cpsn) changes in curvature, differ qualitatively from the pattern observed with changes in head group composition. Irrespective of the changes in curvature, the amphiphiles promote the formation of gA channels, increase the stability of conducting Alm channels and shift the distribution of Alm channel current levels toward higher current levels.

If changes in intrinsic curvature were the only determinant of the changes in channel function, TX100 (and rTX100), on the one hand, and Cpsn, on the other, should produce opposite changes in Alm and gA channel function. The amphiphile's dominant effects on channel function, therefore, must be due to other amphiphile-dependent effects, where changes in channel structure can be ruled because the structurally quite diverse amphiphiles produce little change in the magnitude of the current transitions in Alm, AgA(15) and the enantiomeric $gA^-(13)$ channels. Focusing on the $gA^-(13)$ and AgA(15) channels, the amphiphiles increase both lifetimes and channel formation frequency, with the larger changes in the $gA^-(13)$ as compared to AgA(15) channels (Figures 9 and 10), which shows that their primary effect is to increase bilayer elasticity that results from the reversible partitioning of amphiphiles in lipid bilayers, e.g., [25,26,28]. A similar conclusion was reached by [27] based on studies on the effects of polyunsaturated fatty acids, known promoters of inverted hexagonal phases and negative curvature, e.g., [106].

Amphiphiles may, of course, alter other bilayer properties, including the surface potential associated with the partitioning of charged molecules at the interface [107,108] or the interfacial dipole potential associated with the partitioning of dipolar molecules into the interface [91]; see also [92]. Because Alm function would vary with changes in the electric field within the membrane, we added the amphiphiles to both sides of the membrane to minimize changes in the electric field across the membrane, cf. [93]. We also note that the Alm current levels changed little in the presence of the amphiphiles (Table 1).

Comparing the concentration-dependent effects of the amphiphiles, Cpsn is three-fold less potent than TX100 and rTX100 in producing changes in channel function, whether shifting the gA monomer↔dimer equilibrium to the right or promoting the formation of Alm channels and stabilizing the higher conduction levels in Alm channels. Analyzing the concentration-dependent shifts in the distribution among different Alm current levels (Figures 4 and 5), we further found that the amphiphiles promoted higher current levels, as compared to the lower levels.

The Alm experiments were performed at nominal Alm concentrations ~10^{-8} M (in DOPC membranes, 10-fold higher in the DOPE-containing membranes). Given a partition coefficient of Alm into DOPC membranes, ~1.3×10^3 [109], the Alm/lipid mole fraction in the membrane was ~10^{-5} (average distance between monomers ~250 nm, about two orders of magnitude longer than the decay length for elastic deformation [74,99]), far below the Alm/lipid mole fractions where Alm induces the formation of non-lamellar phases (~10^{-2} [110]), and Huang and colleagues demonstrated the transition from a surface-bound S state to a membrane-inserted I state (~10^{-2} [72]) or the mole fractions used to visualize Alm channels using X-ray scattering (10^{-2}–10^{-1} [77,111]). Whereas the S→I transition described by Huang and colleagues (e.g., [38]) is likely to result from accumulated curvature stress associated with increasing surface density in the S state [72,74], the shift in the distribution of current transitions we observe probably do not result from changes in the curvature stress due to the S state because the mole fraction of Alm in the membranes is so low (average separation between monomers ~250 nm).

Our results do, however, provide insights into molecular features of Alm channels. First, we needed higher concentrations (mole fractions in the membrane) in the experiments with DOPC/DOPE mixtures. This may reflect the weaker binding of Alm to DOPC/DOPE membranes [73] as well as an increased insertion energy of the bilayer-spanning peptide due to Alm-bilayer hydrophobic mismatch [112]. Second, the opposite effects of curvature on Alm and gA channels suggest that the higher Alm channel conductance states have longer hydrophobic lengths than the lower conductance states. Knowing that H_X is negative (text below Equation (10)), the $H_X \cdot (d_0 - l) \cdot c_0$ term in Equation (10) will decrease with increasing l when $c_0 < 0$ (and increase with increasing l when $c_0 > 0$). In the case of gA channels, where $l < d_0$, the $H_X \cdot (d_0 - l) \cdot c_0$ term will increase with decreasing c_0, which likely accounts for the opposite effects of phospholipid head group-dependent changes in curvature on Alm and gA channels.

The similar effects of changes in elasticity on Alm and gA, as evident in Figure 11, likewise can be understood by considering how changes in bilayer elasticity alter ΔG_{def}. Whenever $d_0 \neq l$, the $H_B \cdot (d_0 - l)^2$ term in Equation (10) will be positive and, except for small hydrophobic mismatches, dominate. That is, ΔG_{def} will decrease with increasing bilayer elasticity (decreasing H_B). When amphiphiles partition into bilayer/solution interfaces, they will alter both elasticity [14,24–26,28,87,88] and curvature, e.g., [24]. The amphiphile-induced changes in curvature, however, are modest compared with the changes observed when the head group composition is changed, as evident by comparing Figure 3 in [29], where c_0 varied between -0.104 nm^{-1} in DOPC membranes and -0.468 nm^{-1} in DOPE membranes, with Figure 5 in [24], where c_0 varied between -0.222 nm^{-1} at a TX100 mass fraction of 0.05 (mole fraction $\approx$ 0.08) and -0.258 nm^{-1} at a Cpsn mass fraction of 0.05 (mole fraction $\approx$ 0.14); c_0 was -0.248 in the absence of amphiphile. The changes in head group composition produce a $\Delta c_0 \approx 0.364$ nm^{-1}, which should be compared to the amphiphile-induced changes, $\Delta c_0 \approx 0.036$ nm^{-1}, which provides a mechanistic basis for why the dominant effect of amphiphiles is the increased elasticity that results from their reversible partitioning into the bilayer/solution interface. The energetic consequences of the changes in curvature are modest because the changes in curvature are modest, which provides a mechanism for why amphiphiles have similar effects on Alm and gA channels and why amphiphile-induced changes in membrane protein function appear to be dominated by changes in bilayer elasticity [8,14,24].

4. Materials and Methods

4.1. Materials

1,2-Dioleoyl-*sn*-glycero-3-phosphocholine (DOPC), 1,2-dioleoyl-*sn*-glycero-3-phosphoethanolamine (DOPE) and 1,2-dioleoyl-*sn*-glycero-3-[phospho-L-serine] (DOPS) were from Avanti Polar Lipids (Alabaster, AL, USA) and used without further purification. *n*-Decane was 99.9% pure and from ChemSampCo (Trenton, NJ, USA). Alamethicin (Alm) from *Tricoderma viride* was from Sigma (St. Louis, MO, USA); it was used as supplied. The gramicidin A (gA) analog [Ala^1]gA (AgA(15), with 15 amino acids in the sequence) and the sequence-shortened enantiomeric analog des-(D-Val^1-Gly^2)-gA$^-$ (gA$^-$(13), with 13 amino acids in the sequence) were synthesized and purified as described in [113]; they were 99+% pure, as determined by HPLC. Protein grade Triton X-100 (TX100) and reduced Triton X-100 (rTX100) were from Calbiochem-Novabiochem (La Jolla, CA, USA). Capsaicin (Cpsn) was from ICN Biomedicals (Aurora, OH, USA). Stock solutions of Alm, the gA analogs, TX100, rTX100 and Cpsn were prepared using dimethylsulfoxide (DMSO) (HPLC grade from Burdick & Jackson, Muskegon, MI, USA). The electrolyte solution was 0.1 or 1.0 M NaCl buffered to either pH 7.0 with 10 mM HEPES or pH 4.0 with 10 mM glycine–glycine (plus 1 mM EDTA) from Sigma.

4.2. Methods

Planar lipid bilayers were formed from 2.5% *w*/*v* suspensions of phospholipid in *n*-decane across a 1.5 mm hole in a Teflon® partition separating the two electrolyte solutions, using the pipette method [114]; see also [115]. All experiments were performed at 25 $\pm$ 1 °C. Care was taken to minimize the total amount of lipid (and *n*-decane) that was added; the total volume of the lipid/*n*-decane solution usually was 1000-fold less than the volume of the aqueous solution.

For the Alm experiments, Alm was added to the *trans* side of the lipid bilayer; the *cis* side was the electrical ground. For the experiments with DOPC bilayers, we used ~10^{-8} M (nominal aqueous concentration, not corrected for adsorption of Alm to the bilayer and other surfaces in the chamber); for the experiments with DOPE or DOPS bilayers, we needed a 10-fold higher concentration to observe comparable channel activity. The applied potential was +150 mV.

For the gA experiments, we used the analogs AgA(15) and gA^{-}(13), which allows for a test of how the effects of TX100, rTX100 or Cpsn depends on hydrophobic mismatch [13,24,98]; the applied potential was ±200 mV.

TX100, rTX100 or Cpsn were added to both aqueous solutions (both sides of the bilayer) during stirring as aliquots of 10 mM stock solutions in DMSO (stored at 5 °C). After amphiphile addition, the aqueous phases were stirred for at least 5 min before the measurements resumed. The total amount of added DMSO was less than 0.5% of the volume of the electrolyte solution, a concentration that has no effect on Alm or gA channel function.

The experimental protocol was as follows: after a stable membrane was formed, Alm was added to the *trans* side, or AgA(15) plus gA^{-}(13) were added to both sides of the membrane, and control recordings were obtained. If channel activity was stable, the amphiphile was added by pipette and allowed to equilibrate before measurements resumed. If the membrane and channel activity were stable, another aliquot of the amphiphile was added and allowed to equilibrate, and then measurements resumed. If the membrane or the channel activity were unstable, the experiment was terminated.

Single-channel experiments were conducted using the bilayer-punch method [96] and a Dagan 3900A patch-clamp amplifier (Dagan Corp., Minneapolis, MN, USA) with a 3910 bilayer-expander module. The current signal in the Alm was filtered at 10 kHz, digitized at 20 kHz and digitally filtered at 8 kHz; the current signal in the gA experiments was filtered at 2 kHz, digitized at 20 kHz and digitally filtered at 500 Hz before the single-channel transitions were detected using transition-based algorithm [96] implemented in Visual Basic (Microsoft, Redmond, WA, USA).

5. Conclusions

Despite the different mechanisms of channel formation, the function of Alm and gA channels vary with changes in lipid bilayer composition and material properties (thickness, intrinsic curvature and the associated elastic moduli). Changes in head group composition, which alter curvature without altering elasticity, have opposite effects on Alm and gA channels. Amphiphiles, which alter elasticity with modest changes in curvature, have similar effects on Alm and gA channels, and the changes in the Alm channel function can be predicted from the changes in the gA channel function. This latter result is similar to what was found for other ion channels. That is, ion channels (and other membrane proteins) with different gating mechanisms respond similarly to amphiphile-induced changes in bilayer properties. The magnitude of the bilayer-mediated regulation of membrane protein function will differ among different proteins depending on their structure and the conformational transitions that underlie their function because the bilayer contribution to the free energy difference between different protein conformations is the difference in bilayer deformation energies association with the two conformations.

It is, in this context, important that any (indeed all) of the properties of lipid bilayers—thickness, curvature and their associated elastic moduli, etc.—collectively regulate protein function and that changes in one property are likely to be associated with changes in other properties. Again, this emphasizes the importance of the aggregate effects of these changes, e.g., in terms of the (amphiphile-induced) changes in bilayer deformation energy, which provides a mechanism for understanding the bilayer-mediated regulation of any membrane protein.

Supplementary Materials: The following supporting information can be downloaded at: https://www.mdpi.com/article/10.3390/ijms25052758/s1. References [116–118] are cited in the Supplementary Materials.

Author Contributions: Conceptualization, M.A., R.E.K.II and O.S.A.; methodology, M.A. and O.S.A.; formal analysis, M.A. and O.S.A.; resources, R.E.K.II; data curation, M.A. and O.S.A.; writing—original draft preparation, M.A.; writing—review and editing, M.A., R.E.K.II and O.S.A. visualization,

M.A. and O.S.A.; supervision, O.S.A.; project administration, O.S.A., funding acquisition, R.E.K.II and O.S.A. All authors have read and agreed to the published version of the manuscript.

Funding: This research was supported by grants GM21342 (OSA) and RR15569 (REK) from the National Institutes of Health, Bethesda, MD, USA.

Institutional Review Board Statement: Not applicable.

Informed Consent Statement: Not applicable.

Data Availability Statement: The data presented in this study are available upon request from the corresponding author.

Acknowledgments: We thank Michael J. Bruno, Helgi I. Ingólfsson, Jens A. Lundbæk, Radda Rusinova and Daniel S. Stor for helpful discussions. We dedicate this article to the memory of V. Adrian Parsegian, a giant in membrane biophysics and a pioneer in studies on the bilayer-mediated regulation of ion channel function.

Conflicts of Interest: The authors declare no conflicts of interest. The funders had no role in the design of the study; in the collection, analysis or interpretation of data; in the writing of the manuscript, or in the decision to publish the results.

Abbreviations

Alm	Alamethicin
gA	gramicidin A
AgA(15)	[Ala^1]gramicidin A
gA$^-$(13)	des-Val^1,Gly^2-gramicidin A
Cpsn	Capsaicin
TX100	Triton X-100
rTX100	reduced Triton X-100

References

1. Sandermann, H.J. Regulation of membrane enzymes by lipids. *Biochim. Biophys. Acta* **1978**, *515*, 209–237. [CrossRef]
2. Spector, A.A.; Yorek, M.A. Membrane lipid composition and cellular function. *J. Lipid Res.* **1985**, *26*, 1015–1035. [CrossRef] [PubMed]
3. Bienvenüe, A.; Marie, J.S. Modulation of protein function by lipids. *Curr. Top. Membr.* **1994**, *40*, 319–354.
4. Brown, M.F. Modulation of rhodopsin function by properties of the membrane bilayer. *Chem. Phys. Lipids* **1994**, *73*, 159–180. [CrossRef]
5. Lee, A.G. How lipids and proteins interact in a membrane: A molecular approach. *Mol. Biosyst.* **2005**, *1*, 203–212. [CrossRef] [PubMed]
6. Andersen, O.S.; Koeppe, R.E., II. Bilayer thickness and membrane protein function: An energetic perspective. *Annu. Rev. Biophys. Biomol. Struct.* **2007**, *36*, 107–130. [CrossRef]
7. Marsh, D. Protein modulation of lipids, and vice-versa, in membranes. *Biochim. Biophys. Acta* **2008**, *1778*, 1545–1575. [CrossRef]
8. Lundbæk, J.A.; Collingwood, S.A.; Ingólfsson, H.I.; Kapoor, R.; Andersen, O.S. Lipid bilayer regulation of membrane protein function: Gramicidin channels as molecular force probes. *J. R. Soc. Interface* **2010**, *7*, 373–395. [CrossRef]
9. Szlenk, C.T.; GC, J.B.; Natesan, S. Does the Lipid Bilayer Orchestrate Access and Binding of Ligands to Transmembrane Orthosteric/Allosteric Sites of G Protein-Coupled Receptors? *Mol. Pharmacol.* **2019**, *96*, 527–541. [CrossRef]
10. Levental, K.R.; Malmberg, E.; Symons, J.L.; Fan, Y.Y.; Chapkin, R.S.; Ernst, R.; Levental, I. Lipidomic and biophysical homeostasis of mammalian membranes counteracts dietary lipid perturbations to maintain cellular fitness. *Nat. Commun.* **2020**, *11*, 1339. [CrossRef]
11. Payandeh, J.; Volgraf, M. Ligand binding at the protein-lipid interface: Strategic considerations for drug design. *Nat. Rev. Drug Discov.* **2021**, *20*, 710–722. [CrossRef]
12. Levental, I.; Lyman, E. Regulation of membrane protein structure and function by their lipid nano-environment. *Nat. Rev. Mol. Cell Biol.* **2023**, *24*, 107–122. [CrossRef]
13. Ashrafuzzaman, M.; Lampson, M.A.; Greathouse, D.V.; Koeppe, R.E.I.; Andersen, O.S. Manipulating lipid bilayer material properties using biologically active amphipathic molecules. *J. Phys. Condens. Matter* **2006**, *18*, S1235–S1255. [CrossRef]
14. Rusinova, R.; Herold, K.F.; Sanford, R.L.; Greathouse, D.V.; Hemmings, H.C.J.; Andersen, O.S. Thiazolidinedione insulin sensitizers alter lipid bilayer properties and voltage-dependent sodium channel function: Implications for drug discovery. *J. Gen. Physiol.* **2011**, *138*, 249–270. [CrossRef]

15. Nielsen, C.; Andersen, O.S. Inclusion-induced bilayer deformations: Effects of monolayer equilibrium curvature. *Biophys. J.* **2000**, *79*, 2583–2604. [CrossRef]
16. Hatzakis, N.S.; Bhatia, V.K.; Larsen, J.; Madsen, K.L.; Bolinger, P.Y.; Kunding, A.H.; Castillo, J.; Gether, U.; Hedegard, P.; Stamou, D. How curved membranes recruit amphipathic helices and protein anchoring motifs. *Nat. Chem. Biol.* **2009**, *5*, 835–841. [CrossRef]
17. Iversen, L.; Mathiasen, S.; Larsen, J.B.; Stamou, D. Membrane curvature bends the laws of physics and chemistry. *Nat. Chem. Biol.* **2015**, *11*, 822–825. [CrossRef] [PubMed]
18. Nagle, J.F.; Wiener, M.C. Structure of fully hydrated bilayer dispersions. *Biochim. Biophys. Acta* **1988**, *942*, 1–10. [CrossRef] [PubMed]
19. Kucerka, N.; Tristram-Nagle, S.; Nagle, J.F. Structure of fully hydrated fluid phase lipid bilayers with monounsaturated chains. *J. Membr. Biol.* **2005**, *208*, 193–202. [CrossRef] [PubMed]
20. Rostovtseva, T.K.; Petrache, H.I.; Kazemi, N.; Hassanzadeh, E.; Bezrukov, S.M. Interfacial polar interactions affect gramicidin channel kinetics. *Biophys. J.* **2008**, *94*, L23–L25. [CrossRef] [PubMed]
21. Maer, A.M.; Rusinova, R.; Providence, L.L.; Ingólfsson, H.I.; Collingwood, S.A.; Lundbæk, J.A.; Andersen, O.S. Regulation of Gramicidin Channel Function Solely by Changes in Lipid Intrinsic Curvature. *Front. Physiol.* **2022**, *13*, 836789. [CrossRef]
22. Jung, D.; Powers, J.P.; Straus, S.K.; Hancock, R.E. Lipid-specific binding of the calcium-dependent antibiotic daptomycin leads to changes in lipid polymorphism of model membranes. *Chem. Phys. Lipids* **2008**, *154*, 120–128. [CrossRef] [PubMed]
23. Hakizimana, P.; Masureel, M.; Gbaguidi, B.; Ruysschaert, J.M.; Govaerts, C. Interactions between phosphatidylethanolamine headgroup and LmrP, a multidrug transporter: A conserved mechanism for proton gradient sensing? *J. Biol. Chem.* **2008**, *283*, 9369–9376. [CrossRef] [PubMed]
24. Lundbæk, J.A.; Birn, P.; Tape, S.E.; Toombes, G.E.; Søgaard, R.; Koeppe, R.E., II; Gruner, S.M.; Hansen, A.J.; Andersen, O.S. Capsaicin regulates voltage-dependent sodium channels by altering lipid bilayer elasticity. *Mol. Pharmacol.* **2005**, *68*, 680–689. [CrossRef] [PubMed]
25. Evans, E.; Rawicz, W.; Hofmann, A.F. Lipid bilayer expansion and mechanical disruption in solutions of water-soluble bile acid. In *Bile Acids in Gastroenterology: Basic and Clinical Advances*; Hofmann, A.F., Paumgartner, G., Stiehl, A., Eds.; Kluwer Academic Publishers: Dordrecht, The Netherlands, 1995; pp. 59–68.
26. Zhelev, D.V. Material property characteristics for lipid bilayers containing lysolipid. *Biophys. J.* **1998**, *75*, 321–330. [CrossRef] [PubMed]
27. Bruno, M.J.; Koeppe, R.E., II; Andersen, O.S. Docosahexaenoic acid alters bilayer elastic properties. *Proc. Natl. Acad. Sci. USA* **2007**, *104*, 9638–9643. [CrossRef] [PubMed]
28. Bruno, M.J.; Rusinova, R.; Gleason, N.J.; Koeppe, R.E., II; Andersen, O.S. Interactions of drugs and amphiphiles with membranes: Modulation of lipid bilayer elastic properties by changes in acyl chain unsaturation and protonation. *Faraday Disc.* **2013**, *161*, 461–480. [CrossRef]
29. Keller, S.L.; Bezrukov, S.M.; Gruner, S.M.; Tate, M.W.; Vodyanoy, I.; Parsegian, V.A. Probability of alamethicin conductance states varies with nonlamellar tendency of bilayer phospholipids. *Biophys. J.* **1993**, *65*, 23–27. [CrossRef]
30. Lundbæk, J.A.; Maer, A.M.; Andersen, O.S. Lipid bilayer electrostatic energy, curvature stress, and assembly of gramicidin channels. *Biochemistry* **1997**, *36*, 5695–5701. [CrossRef]
31. Lundbæk, J.A.; Birn, P.; Girshman, J.; Hansen, A.J.; Andersen, O.S. Membrane stiffness and channel function. *Biochemistry* **1996**, *35*, 3825–3830. [CrossRef]
32. Kleinkauf, H.; Von Döhren, H. A nonribosomal system of peptide biosynthesis. *Eur. J. Biochem.* **1996**, *236*, 335–351. [CrossRef] [PubMed]
33. Bezrukov, S.M. Functional consequences of lipid packing stress. *Curr. Opin. Colloid Interface Sci.* **2000**, *5*, 237–243. [CrossRef]
34. Sarges, R.; Witkop, B.; Gramicidin, A.V. The structure of valine- and isoleucine-gramicidin A. *J. Am. Chem. Soc.* **1965**, *87*, 2011–2019. [CrossRef]
35. Abo-Riziq, A.; Crews, B.O.; Callahan, M.P.; Grace, L.; de Vries, M.S. Spectroscopy of isolated gramicidin peptides. *Angew. Chem. Int. Ed. Engl.* **2006**, *45*, 5166–5169. [CrossRef]
36. O'Connell, A.M.; Koeppe, R.E., II; Andersen, O.S. Kinetics of gramicidin channel formation in lipid bilayers: Transmembrane monomer association. *Science* **1990**, *250*, 1256–1259. [CrossRef]
37. Rinehart, K.L.J.; Cook, J.C.J.; Meng, H.; Olson, K.L.; Pandey, R.C. Mass spectrometric determination of molecular formulas for membrane-modifying antibiotics. *Nature* **1977**, *269*, 832–833. [CrossRef]
38. Huang, H.W. Molecular mechanism of antimicrobial peptides: The origin of cooperativity. *Biochim. Biophys. Acta* **2006**, *1758*, 1292–1302. [CrossRef] [PubMed]
39. Bamberg, E.; Läuger, P. Channel formation kinetics of gramicidin A in lipid bilayer membranes. *J. Membr. Biol.* **1973**, *11*, 177–194. [CrossRef]
40. Zingsheim, H.P.; Neher, E. The equivalence of fluctuation analysis and chemical relaxation measurements: A kinetic study of ion pore formation in thin lipid membranes. *Biophys. Chem.* **1974**, *2*, 197–207. [CrossRef]
41. Veatch, W.R.; Mathies, R.; Eisenberg, M.; Stryer, L. Simultaneous fluorescence and conductance studies of planar bilayer membranes containing a highly active and fluorescent analog of gramicidin A. *J. Mol. Biol.* **1975**, *99*, 75–92. [CrossRef]
42. Hickok, N.J.; Kustin, K.; Veatch, W. Relaxation spectra of gramicidin dimerization in a lipid bilayer membrane. *Biochim. Biophys. Acta* **1986**, *858*, 99–106. [CrossRef] [PubMed]

43. Rokitskaya, T.I.; Antonenko, Y.N.; Kotova, E.A. Photodynamic inactivation of gramicidin channels: A flash-photolysis study. *Biochim. Biophys. Acta* **1996**, *1275*, 221–226. [CrossRef] [PubMed]
44. Lum, K.; Ingólfsson, H.I.; Koeppe, R.E., II; Andersen, O.S. Exchange of Gramicidin between Lipid Bilayers: Implications for the Mechanism of Channel Formation. *Biophys. J.* **2017**, *113*, 1757–1767. [CrossRef] [PubMed]
45. Arseniev, A.S.; Barsukov, I.L.; Bystrov, V.F.; Ovchinnikov, Y.A. Spatial structure of a gramicidin A transmembrane ion channel. NMR analysis in micelles. *Biol. Membr.* **1986**, *3*, 437–462.
46. Townsley, L.E.; Tucker, W.A.; Sham, S.; Hinton, J.F. Structures of gramicidins A, B, and C incorporated into sodium dodecyl sulfate micelles. *Biochemistry* **2001**, *40*, 11676–11686. [CrossRef] [PubMed]
47. Ketchem, R.R.; Hu, W.; Cross, T.A. High-resolution conformation of gramicidin A in a lipid bilayer by solid-state NMR. *Science* **1993**, *261*, 1457–1460. [CrossRef] [PubMed]
48. Ketchem, R.; Roux, B.; Cross, T. High-resolution polypeptide structure in a lamellar phase lipid environment from solid state NMR derived orientational constraints. *Structure* **1997**, *5*, 1655–1669. [CrossRef]
49. Allen, T.W.; Andersen, O.S.; Roux, B. Structure of gramicidin a in a lipid bilayer environment determined using molecular dynamics simulations and solid-state NMR data. *J. Am. Chem. Soc.* **2003**, *125*, 9868–9877. [CrossRef]
50. Greathouse, D.V.; Hinton, J.F.; Kim, K.S.; Koeppe, R.E., II. Gramicidin A/short-chain phospholipid dispersions: Chain length dependence of gramicidin conformation and lipid organization. *Biochemistry* **1994**, *33*, 4291–4299. [CrossRef]
51. Mobashery, N.; Nielsen, C.; Andersen, O.S. The conformational preference of gramicidin channels is a function of lipid bilayer thickness. *FEBS Lett.* **1997**, *412*, 15–20. [CrossRef]
52. Galbraith, T.P.; Wallace, B.A. Phospholipid chain length alters the equilibrium between pore and channel forms of gramicidin. *Faraday Discuss.* **1998**, *111*, 159–164; discussion 225–246. [CrossRef] [PubMed]
53. Höfer, N.; Aragão, D.; Caffrey, M. Crystallizing transmembrane peptides in lipidic mesophases. *Biophys. J.* **2010**, *99*, L23–L25. [CrossRef] [PubMed]
54. Wallace, B.A.; Veatch, W.R.; Blout, E.R. Conformation of gramicidin A in phospholipid vesicles: Circular dichroism studies of effects of ion binding, chemical modification, and lipid structure. *Biochemistry* **1981**, *20*, 5754–5760. [CrossRef] [PubMed]
55. Katsaras, J.; Prosser, R.S.; Stinson, R.H.; Davis, J.H. Constant helical pitch of the gramicidin channel in phospholipid bilayers. *Biophys. J.* **1992**, *61*, 827–830. [CrossRef] [PubMed]
56. Busath, D.D.; Andersen, O.S.; Koeppe, R.E., II. On the conductance heterogeneity in membrane channels formed by gramicidin A. A cooperative study. *Biophys. J.* **1987**, *51*, 79–88. [CrossRef] [PubMed]
57. Hladky, S.B.; Haydon, D.A. Ion transfer across lipid membranes in the presence of gramicidin A. I. Studies of the unit conductance channel. *Biochim. Biophys. Acta* **1972**, *274*, 294–312. [CrossRef] [PubMed]
58. Kolb, H.A.; Bamberg, E. Influence of membrane thickness and ion concentration on the properties of the gramicidin a channel. Autocorrelation, spectral power density, relaxation and single-channel studies. *Biochim. Biophys. Acta.* **1977**, *464*, 127–141. [CrossRef]
59. Elliott, J.R.; Needham, D.; Dilger, J.P.; Haydon, D.A. The effects of bilayer thickness and tension on gramicidin single-channel lifetime. *Biochim. Biophys. Acta* **1983**, *735*, 95–103. [CrossRef]
60. Huang, H.W. Deformation free energy of bilayer membrane and its effect on gramicidin channel lifetime. *Biophys. J.* **1986**, *50*, 1061–1070. [CrossRef]
61. Beaven, A.H.; Maer, A.M.; Sodt, A.J.; Rui, H.; Pastor, R.W.; Andersen, O.S.; Im, W. Gramicidin A Channel Formation Induces Local Lipid Redistribution I: Experiment and Simulation. *Biophys. J.* **2017**, *112*, 1185–1197. [CrossRef]
62. Sodt, A.J.; Beaven, A.H.; Andersen, O.S.; Im, W.; Pastor, R.W. Gramicidin A Channel Formation Induces Local Lipid Redistribution II: A 3D Continuum Elastic Model. *Biophys. J.* **2017**, *112*, 1198–1213. [CrossRef] [PubMed]
63. Gordon, L.G.M.; Haydon, D.A. The unit conductance channel of alamethicin. *Biochim. Biophys. Acta* **1972**, *255*, 1014–1018. [CrossRef] [PubMed]
64. Boheim, G. Statistical analysis of alamethicin channels in black lipid membranes. *J. Membr. Biol.* **1974**, *19*, 277–303. [CrossRef] [PubMed]
65. Latorre, R.; Alvarez, O. Voltage-dependent channels in planar lipid bilayer membranes. *Physiol. Rev.* **1981**, *61*, 77–150. [CrossRef] [PubMed]
66. Woolley, G.A.; Dunn, A.; Wallace, B.A. Gramicidin-lipid interactions induce specific tryptophan side-chain conformations. *Biochem. Soc. Trans.* **1992**, *20*, 864–867. [CrossRef] [PubMed]
67. Cafiso, D.S. Alamethicin: A peptide model for voltage gating and protein-membrane interactions. *Annu. Rev. Biophys. Biomol. Struct.* **1994**, *23*, 141–165. [CrossRef] [PubMed]
68. Bechinger, B. The structure, dynamics and orientation of antimicrobial peptides in membranes by multidimensional solid-state NMR spectroscopy. *Biochim. Biophys. Acta* **1999**, *1462*, 157–183. [CrossRef] [PubMed]
69. Fox, R.O.J.; Richards, F.M. A voltage-gated ion channel model inferred from the crystal structure of alamethicin at 1.5-Å resolution. *Nature* **1982**, *300*, 325–330. [CrossRef]
70. Archer, S.J.; Ellena, J.F.; Cafiso, D.S. Dynamics and aggregation of the peptide ion channel alamethicin. Measurements using spin-labeled peptides. *Biophys. J.* **1991**, *60*, 389–398. [CrossRef]
71. Huang, H.W.; Wu, Y. Lipid-alamethicin interactions influence alamethicin orientation. *Biophys. J.* **1991**, *60*, 1079–1087. [CrossRef]

72. Chen, F.Y.; Lee, M.T.; Huang, H.W. Evidence for membrane thinning effect as the mechanism for peptide-induced pore formation. *Biophys. J.* **2003**, *84*, 3751–3758. [CrossRef]
73. Lewis, J.R.; Cafiso, D.S. Correlation between the free energy of a channel-forming voltage-gated peptide and the spontaneous curvature of bilayer lipids. *Biochemistry* **1999**, *38*, 5932–5938. [CrossRef]
74. Huang, H.W. Elasticity of lipid bilayer interacting with amphiphilic helical peptides. *J. Phys. II* **1995**, *5*, 1427–1431. [CrossRef]
75. He, K.; Ludtke, S.J.; Worcester, D.L.; Huang, H.W. Neutron scattering in the plane of membranes: Structure of alamethicin pores. *Biophys. J.* **1996**, *70*, 2659–2666. [CrossRef]
76. Qian, S.; Wang, W.; Yang, L.; Huang, H.W. Structure of the alamethicin pore reconstructed by x-ray diffraction analysis. *Biophys. J.* **2008**, *94*, 3512–3522. [CrossRef]
77. Pan, J.; Tieleman, D.P.; Nagle, J.F.; Kucerka, N.; Tristram-Nagle, S. Alamethicin in lipid bilayers: Combined use of X-ray scattering and MD simulations. *Biochim. Biophys. Acta* **2009**, *1788*, 1387–1397. [CrossRef]
78. Baumann, G.; Mueller, P. A molecular model of membrane excitability. *J. Supramol. Struct.* **1974**, *2*, 538–557. [CrossRef]
79. Opsahl, L.R.; Webb, W.W. Transduction of membrane tension by the ion channel alamethicin. *Biophys. J.* **1994**, *66*, 71–74. [CrossRef] [PubMed]
80. Bezrukov, S.M.; Vodyanoy, I. Probing alamethicin channels with water-soluble polymers. Effect on conductance of channel states. *Biophys. J.* **1993**, *64*, 16–25. [CrossRef] [PubMed]
81. He, K.; Ludtke, S.J.; Huang, H.W.; Worcester, D.L. Antimicrobial peptide pores in membranes detected by neutron in-plane scattering. *Biochemistry* **1995**, *34*, 15614–15618. [CrossRef] [PubMed]
82. Bak, M.; Bywater, R.P.; Hohwy, M.; Thomsen, J.K.; Adelhorst, K.; Jakobsen, H.J.; Sorensen, O.W.; Nielsen, N.C. Conformation of alamethicin in oriented phospholipid bilayers determined by ^{15}N solid-state nuclear magnetic resonance. *Biophys. J.* **2001**, *81*, 1684–1698. [CrossRef]
83. Rizzo, V.; Schwarz, G.; Voges, K.P.; Jung, G. Molecular shape and dipole moment of alamethicin-like synthetic peptides. *Eur. Biophys. J.* **1985**, *12*, 67–73. [CrossRef] [PubMed]
84. Hanke, W.; Boheim, G. The lowest conductance state of the alamethicin pore. *Biochim. Biophys. Acta* **1980**, *596*, 456–462. [CrossRef] [PubMed]
85. Bezrukov, S.M.; Rand, R.P.; Vodyanoy, I.; Parsegian, V.A. Lipid packing stress and polypeptide aggregation: Alamethicin channel probed by proton titration of lipid charge. *Faraday Discuss.* **1998**, *111*, 173–183; discussion 225–246. [CrossRef] [PubMed]
86. Ly, H.V.; Longo, M.L. The influence of short-chain alcohols on interfacial tension, mechanical properties, area/molecule, and permeability of fluid lipid bilayers. *Biophys. J.* **2004**, *87*, 1013–1033. [CrossRef]
87. Lundbæk, J.A.; Koeppe, R.E., II; Andersen, O.S. Amphiphile regulation of ion channel function by changes in the bilayer spring constant. *Proc. Natl. Acad. Sci. USA* **2010**, *107*, 15427–15430. [CrossRef]
88. Kapoor, R.; Peyear, T.A.; Koeppe, R.E., II; Andersen, O.S. Antidepressants are modifiers of lipid bilayer properties. *J. Gen. Physiol.* **2019**, *151*, 342–356. [CrossRef] [PubMed]
89. Lundbæk, J.A.; Birn, P.; Hansen, A.J.; Søgaard, R.; Nielsen, C.; Girshman, J.; Bruno, M.J.; Tape, S.E.; Egebjerg, J.; Greathouse, D.V.; et al. Regulation of sodium channel function by bilayer elasticity: The importance of hydrophobic coupling. Effects of Micelle-forming amphiphiles and cholesterol. *J. Gen. Physiol.* **2004**, *123*, 599–621. [CrossRef] [PubMed]
90. Søgaard, R.; Werge, T.M.; Bertelsen, C.; Lundbye, C.; Madsen, K.L.; Nielsen, C.H.; Lundbæk, J.A. $GABA_A$ receptor function is regulated by lipid bilayer elasticity. *Biochemistry* **2006**, *45*, 13118–13129. [CrossRef]
91. Andersen, O.S.; Finkelstein, A.; Katz, I.; Cass, A. Effect of phloretin on the permeability of thin lipid membranes. *J. Gen. Physiol.* **1976**, *67*, 749–771. [CrossRef]
92. Duffin, R.L.; Garrett, M.P.; Busath, D.D. Modulation of Lipid Bilayer Interfacial Dipole Potential by Phloretin, RH421, and 6-Ketocholestanol as Probed by Gramicidin Channel Conductance. *Langmuir* **2003**, *19*, 1439–1442. [CrossRef]
93. Mereuta, L.; Asandei, A.; Luchian, T. Meet me on the other side: Trans-bilayer modulation of a model voltage-gated ion channel activity by membrane electrostatics asymmetry. *PLoS ONE* **2011**, *6*, e25276. [CrossRef]
94. Colquhoun, D.; Sigworth, F.J. Fitting and statistical analysis of single-channel records. In *Single-Channel Recording*, 2nd ed.; Sakmann, B., Neher, E., Eds.; Plenum Press: New York, NY, USA, 1995; pp. 483–587.
95. Sawyer, D.B.; Koeppe, R.E., II; Andersen, O.S. Induction of conductance heterogeneity in gramicidin channels. *Biochemistry* **1989**, *28*, 6571–6583. [CrossRef]
96. Andersen, O.S. Ion movement through gramicidin A channels. Single-channel measurements at very high potentials. *Biophys. J.* **1983**, *41*, 119–133. [CrossRef] [PubMed]
97. Ingólfson, H.; Kapoor, R.; Collingwood, S.A.; Andersen, O.S. Single molecule methods for monitoring changes in bilayer elastic properties. *J. Vis. Exp.* **2008**, *21*, e1032.
98. Artigas, P.; Al'aref, S.J.; Hobart, E.A.; Diaz, L.F.; Sakaguchi, M.; Straw, S.; Andersen, O.S. 2,3-Butanedione monoxime affects Cystic Fibrosis Transmembrane Conductance Regulator channel function through phosphorylation-dependent and phosphorylation-independent mechanisms: The role of bilayer material properties. *Mol. Pharmacol.* **2006**, *70*, 2015–2026. [CrossRef]
99. Nielsen, C.; Goulian, M.; Andersen, O.S. Energetics of inclusion-induced bilayer deformations. *Biophys. J.* **1998**, *74*, 1966–1983. [CrossRef]
100. Lundbæk, J.A.; Andersen, O.S. Spring constants for channel-induced lipid bilayer deformations—Estimates using gramicidin channels. *Biophys. J.* **1999**, *76*, 889–895. [CrossRef]

101. White, S.H.; Thompson, T.E. Capacitance, area, and thickness variations in thin lipid films. *Biochim. Biophys. Acta* **1973**, *323*, 7–22. [CrossRef] [PubMed]
102. White, S.H. Comments on "electrical breakdown of bimolecular lipid membranes as an electromechanical instability". *Biophys. J.* **1974**, *14*, 155–158. [CrossRef]
103. Evans, E.A.; Simon, S. Mechanics of electrocompression of lipid bilayer membranes. *Biophys. J.* **1975**, *15*, 850–852. [CrossRef]
104. Requena, J.; Haydon, D.A.; Hladky, S.B. Lenses and the compression of black lipid membranes by an electric field. *Biophys. J.* **1975**, *15*, 77–81.
105. Rusinova, R.; Koeppe, R.E., II; Andersen, O.S. A general mechanism for drug promiscuity: Studies with amiodarone and other antiarrhythmics. *J. Gen. Physiol.* **2015**, *146*, 463–475. [CrossRef] [PubMed]
106. Tate, M.W.; Eikenberry, E.F.; Turner, D.C.; Shyamsunder, E.; Gruner, S.M. Nonbilayer phases of membrane lipids. *Chem. Phys. Lipids* **1991**, *57*, 147–164. [CrossRef]
107. McLaughlin, S. Salicylates and phospholipid bilayer membranes. *Nature* **1973**, *243*, 234–236. [CrossRef] [PubMed]
108. McLaughlin, S.; Harary, H. The hydrophobic adsorption of charged molecules to bilayer membranes: A test of the applicability of the Stern equation. *Biochemistry* **1976**, *15*, 1941–1948. [CrossRef] [PubMed]
109. Schwarz, G.; Stankowski, S.; Rizzo, V. Thermodynamic analysis of incorporation and aggregation in a membrane: Application to the pore-forming peptide alamethicin. *Biochim. Biophys. Acta* **1986**, *861*, 141–151. [CrossRef] [PubMed]
110. Keller, S.L.; Gruner, S.M.; Gawrisch, K. Small concentrations of alamethicin induce a cubic phase in bulk phosphatidylethanolamine mixtures. *Biochim. Biophys. Acta* **1996**, *1278*, 241–246. [CrossRef] [PubMed]
111. He, K.; Ludtke, S.J.; Heller, W.T.; Huang, H.W. Mechanism of alamethicin insertion into lipid bilayers. *Biophys. J.* **1996**, *71*, 2669–2679. [CrossRef]
112. Pan, J.; Tristram-Nagle, S.; Nagle, J.F. Alamethicin aggregation in lipid membranes. *J. Membr. Biol.* **2009**, *231*, 11–27. [CrossRef]
113. Greathouse, D.V.; Koeppe, R.E., II; Providence, L.L.; Shobana, S.; Andersen, O.S. Design and characterization of gramicidin channels. *Methods Enzymol.* **1999**, *294*, 525–550. [PubMed]
114. Szabo, G.; Eisenman, G.; Ciani, S. The effects of macrotetralide actin antibiotics on the electrical properties of phospholipid bilayer membranes. *J. Membr. Biol.* **1969**, *1*, 346–382. [CrossRef] [PubMed]
115. Kapoor, R.; Kim, J.H.; Ingolfson, H.; Andersen, O.S. Preparation of artificial bilayers for electrophysiology experiments. *J. Vis. Exp.* **2008**, *20*, e1033.
116. de Kroon, A.I.P.M.; Timmermans, J.W.; Killian, J.A.; de Kruijff, B. The pH dependence of headgroup and acyl chain structure and dynamics of phosphatidylserine, studied by 2H-NMR. *Chem. Phys. Lipids* **1990**, *54*, 33–42. [CrossRef]
117. Fuller, N.; Benatti, C.R.; Rand, R.P. Curvature and bending constants for phosphatidylserine-containing membranes. *Biophys. J.* **2003**, *85*, 1667–1674. [CrossRef]
118. Aguilella, V.M.; Bezrukov, S.M. Alamethicin channel conductance modified by lipid charge. *Eur. Biophys. J.* **2001**, *30*, 233–241.